# DYNAMIC MODELING OF AN ORGANIC RANKINE CYCLE

by

Hasan Börke Birgin

B.S., Civil Engineering, Bogaziçi University, 2015

Submitted to the Institute for Graduate Studies in
Science and Engineering in partial fulfillment of
the requirements for the degree of
Master of Science

Graduate Program in Civil Engineering

Boğaziçi University

2018

DYNAMIC MODELING OF AN ORGANIC RANKINE CYCLE

APPROVED BY:

| | |
|---|---|
| Prof. Hilmi Luş<br>(Thesis Supervisor) | ..... |
| Assoc. Prof. Hasan Bedir<br>(Thesis Co-supervisor) | ..... |
| Prof. Günay Anlaş | ..... |
| Prof. Kunt Atalık | ..... |
| Assist. Prof. Hatice Mercan | ..... |

DATE OF APPROVAL: 08.01.2018

# ACKNOWLEDGEMENTS

First of all, I would like to thank my family for supporting me during the entire study. Especially I am thankful to my sister, Birge Birgin, for her presence whenever I need, and endless help on every subject matter.

I would like to express my immense gratefulness to my thesis supervisor Prof. Hilmi Luş, because of his patience, persistent guidance and knowledge. He always steered me to the accurate direction during my entire study.

I am indebted to Assoc. Prof. Hasan Bedir for his unique guidance. He has enlightened me whenever I needed.

I am particularly thankful to Prof. Gülay Altay, she always motivated and encouraged me during my undergraduate and graduate life.

I am also thankful to my colleagues, Fırat Yolaçan and M. Fethi Güllü, for their continuous support and friendship.

# ABSTRACT

## DYNAMIC MODELING OF AN ORGANIC RANKINE CYCLE

A numerical model of an ORC (Organic Rankine Cycle) based on MATLAB environment is constructed in this study. The main components of the ORC are pump, evaporator, turbine and condenser. The organic working fluid (r134a) with low saturation temperature is employed. The low saturation temperature enables organic fluid to change it's phase with low heat input, thus system gains high amount of enthalpy without having excessive heat source. Waste heat and solar collectors are some popular heat sources for ORC's. System design and component selections are made according to steady state operating condition. However, when a disturbance appears, one can not calculate the response of the system based on the steady state model. Hence, it is important to utilize a dynamic model of the energy system. Apart from disturbances, start-up and shut-down phases of the system have also transient outcomes. To define those transients in a thermodynamic cycle is a developing topic. The transient model is employed for the heat exchangers of the system. The turbine and the pump are modeled in the steady state. The effect of variable pressure on the fluid density is considered as instantly. Discretization of the heat exchangers is carried out according to the backward Euler formulation, and implicit scheme of time integration is employed in the model. Between time steps, an iterative solution method is introduced for guessing the spatial distribution of the mass flow rate. Different correlations are presented for the heat transfer in a plate heat exchanger. The examination of the dynamic model is made with constructed steady state heat exchanger model and with the data acquired from the experiment, which is conducted in BURET Laboratory at the Bogazici University Kilyos Campus. The dynamic model can be considered as a reliable predictor of outcomes, when system has disturbances or when system is in a transition.

# ÖZET

## ORGANİK RANKINE ÇEVRİMİ'NİN DİNAMİK MODELLENMESİ

Bu çalışmada, Organik Rankine Çevrimi'nin (ORC) MATLAB üzerinde sayısal bir modeli oluşturulmuştur. ORC'nin ana bileşenleri pompa, evaporatör, türbin ve kondenserdir. Çevrim içerisinde düşük kaynama noktasına sahip organik akışkan kullanılır. Düşük kaynama noktası, organik akışkanın düşük ısı girişi ile buharlaşmasını sağlar, böylece sistem aşırı ısı kaynağına ihtiyaç duymadan entalpi kazanır. Atık ısı ve güneş kolektörleri, ORC'ler için kullanılan ısı kaynaklarıdır. Enerji sistemleri durağan durumda çalışmak için tasarlanırlar. Sistem tasarımı ve bileşen seçimleri, bu durağan durum çalışma koşullarına göre yapılır. Eğer durağan durumdan çıkılırsa, durağan durum modeline dayalı olarak oluşturulan model, sistemin geçişken verilerini hesaplayamaz. Dolayısıyla bir enerji sisteminin dinamik bir modelinin oluşturulması önemlidir. Özellikle sistemin başlangıç ve kapanış zamanlarında ortaya çıkan geçişken sonuçların gözlenmesi, istenilen durağan duruma ulaşılmasını ve sistemin optimum kullanımını sağlar. Termodinamik bir çevrimde bu sonuçların numerik bir model üzerinden gözlemlenmesi henüz gelişmekte olan bir konudur. Oluşturulan modelde, eşanjörler, tepki sürelerinin pompa ve türbine kıyasla uzun olduğu için dinamik olarak modellenmiştir. Bu modelde değişen sistem basıncının akışkan yoğunluğuna olan etkisi anlık olarak kabul edilmiştir. Nümerik model, sonlu hacimler yaklaşımına göre oluşturulmuştur. Zaman adımları arasında, organik akışkanın debisinin uzaysal dağılımını hesaplamak için yinelemeli çözüm yöntemi geliştirilmiştir. Plakalı ısı eşanjöründeki ısı transferini hesaplamak için literatürden çeşitli korelasyonlar sunulmuştur. Dinamik modelin analizi, Boğaziçi Üniversitesi BURET Laboratuvarı'nda yapılan deneyden elde edilen verilerle yapılmıştır. Oluşturulan sayısal durağan durum modeli ile de dinamik modelin hesaplanan çalışma koşullarına yaklaştığı gözlemlenmiştir.

# TABLE OF CONTENTS

# LIST OF FIGURES

# LIST OF TABLES

# LIST OF SYMBOLS

| | |
|---|---|
| $A$ | Cross sectional Area |
| $A_{tr}$ | Heat transfer Area |
| $B$ | Cross sectional Perimeter |
| $C$ | Heat capacity |
| $c$ | Specific heat at constant pressure |
| $D$ | Cross sectional diameter |
| $D_p$ | Port diameter |
| $dl$ | Infinitesimal length |
| $dt$ | Infinitesimal time |
| $en$ | Enter |
| $ex$ | Exit |
| $fin$ | Final |
| $g$ | Gravity |
| $G_t$ | Mass velocity of total flow |
| $gs$ | Gas state |
| $H$ | Enthalpy |
| $h$ | Specific enthalpy |
| $hyd$ | Hydraulic |
| $I$ | Heat transfer coefficient |
| $ini$ | Initial |
| $k$ | Thermal conductivity |
| $L$ | Length of pass |
| $l_h$ | Horizontal port distance |
| $l_v$ | Vertical port distance |
| $L_h$ | Heigth of plate |
| $L_p$ | Pitch between two plates (center to center) |
| $L_w$ | Width of plate |
| $lq$ | Liquid state |

| | |
|---|---|
| $m$ | Mass |
| $\dot{m}$ | Mass flow rate |
| $max$ | Maximum |
| $min$ | Minimum |
| $Nu$ | Nusselt Number |
| $old$ | Old |
| $p$ | Pressure |
| $pass$ | Passing inside heat exchanger |
| $pl$ | Plate |
| $Pr$ | Prandtl Number |
| $Re$ | Reynolds Number |
| $q$ | Heat |
| $sys$ | System |
| $T$ | Temperature |
| $t_p$ | Plate thickness |
| $tr$ | Transfer |
| $u$ | Specific energy |
| $V$ | Volume |
| $Y$ | Latent heat |
| $W$ | Work |
| $v$ | Velocity |
| $\bar{v}$ | Mean velocity of flow |
| | |
| $\Delta T$ | Temperature difference |
| $\varepsilon$ | Effectiveness |
| $\kappa$ | Quality of flow |
| $\mu$ | Dynamic viscosity |
| $\rho$ | Density |
| $\theta$ | Overall heat transfer coefficient |

| | |
|---|---|
| $-$ | Arithmatical average over Control Volume |
| $\sim$ | Integral average over Control Volume |
| $*$ | Iterative |

# LIST OF ACRONYMS/ABBREVIATIONS

| | |
|---|---|
| HEX | Heat Exchanger |
| NTU | Number of transfer units |
| ORC | Organic Rankine Cycle |
| PHE | Plate heat exchanger |
| SS | Steady State |
| TP | Two Phase |

# 1. INTRODUCTION

Organic Rankine Cycle (ORC) applications are increasing their popularity in recent years. Having an organic substance with boiling temperature lower than water as the working fluid, ORCs enable one to produce energy from low temperature sources like solar ponds, geothermal heat and waste heat.

Power cycles generally operate in steady state conditions. It should be emphasized, however, that it is very important to set initial conditions appropriately to reach a desired steady state level. Moreover, for the critical phases of start-up and shut-down, prediction of transient behavior may be very useful. In particular, initializing the mass flow rates of the hot/cold/working fluids in the ORC system according to their initial temperatures is crucial if the power plant is to reach a particular steady state. Based on these considerations, a dynamic model is expected to play a significant part in optimal operations of an ORC.

There are various studies in the literature about dynamic modeling of ORCs which differ from each other by system model (moving boundary, discretized, lumped parameters), by correlations and/or by formulation (log mean temperature difference, NTU-effectiveness). Amongst the components in ORC systems, heat exchangers (evaporators, condensers and chillers) dominate the transient dynamics, since the overall system lag is caused by their thermal response. The system lag is defined as the time between the change in an input and observation of its corresponding effect on the system. Modeling the transient dynamics of exchangers means that one should not only be able to solve for heat transfer between fluids when working fluid is single-phase but also when the working fluid is two-phase (liquid - gas). Constructing an ORC system model requires integration of different subtopics such as dynamic model theory of energy systems, selection of heat transfer correlations according to flow properties, general modeling of heat exchangers, and models of the particular heat exchangers according to type and geometry.

## 1.1. Literature review

### 1.1.1. Transient Models of an Energy Cycle

An energy system is the integrated cooperation of the components such as heat exchangers, power generators and pumps to produce power from the heat input. The dynamic model of an energy system comprises transient models of those components. These components are generally connected in series so that the output from one component acts as the input to another. Such a complex transient system may require large computational power and therefore an analysis to determine those components that dominate the general transient action is extremely beneficial. If the transient dynamics of a certain component has no significant bearing on the transient behavior of the whole system, lumped models can be utilized for that component to significantly decrease computational time.

The simulation of the transient system dynamics require the computation of the time histories of output parameters via solving the governing equations. Although commercial computer programs that can deal with such systems exist, manually constructed simulations are more flexible and suitable for particular applications, and this is the approach that is followed in this work. When the problem is formulated computationally, an initial choice must be made regarding whether to use a moving boundary model or a discretized model. In the former, a partitioning based on energy considerations imposes predefined thermodynamic state zones, whose existence and dimensions are then investigated. In the latter, the thermodynamic state variables are introduced and the general state of the disecretized domain is defined using these variable through the governing equations. In both cases, the constructed transient models should obey both continuity laws and thermodynamic state equations. In this work the discretized model approach is chosen because of its generality and flexibility.

In the following sections of this introductory chapter, details of a variety of available dynamic models of the organic Rankine cycles in the literature are given.

### 1.1.2. Dynamic Model of an Organic Rankine Cycle

The organic Rankine cycles are a specific kind of Rankine cycles. An organic fluid is employed in the Rankine cycle to achieve power generation even for the relatively low heat sources, which is due to the lower saturation temperature of the organic fluid comparing to the water. The popular organic fluids are the refrigerants r245fa and r134a, while Rankine cycle operates with steam (water).

In their study on dynamic modeling and simulation of ORCs, Wei *et al.* [1] propose two alternative formulations to represent the evaporator and the condenser: a moving boundary model and a discrete model. The model of turbine is derived from its map, and, the pump model is constructed based on performance data that is supplied from the manufacturer. The estimated time for the pump and the turbine to reach steady state condition from transient condition is expected to be instant, and therefore static lumped models employed for them. Finite difference approximations are used for discretization of mass, momentum and energy equations. The mass flow rate is not constant through the simulation, an average value of the mass flow rate is scoped and compared with the experimental results. For heat transfer correlations, Gnielinski equation [2] is employed for the single phase zones, and a correlation from W*ä*rmeatlas [3] is used in the two-phase zones for convective heat transfer in an horizontal tube. According to analysis and validation, prediction errors remain about 4%.

Quoilin *et al.* [4] study dynamic modeling of and optimal control strategy for waste heat recovery ORC. Modelica environment is used for simulation, and fluid properties are taken from Fluidprop, which is a commercial computer program for calculating thermodynamic properties of fluids. The study focuses mainly on the evaporator, which is constructed as a single pass heat exchanger. The finite volume method is used to discretize mass and energy conservation equations. For the heat transfer coefficient they defined three values according to the state of the fluid. The linear interpolation is then employed for the transition between two heat transfer coefficients. Other components of the ORC system, namely the expander, the condenser and the pump, are modeled

in steady state conditions since the main focus is on the evaporator. A constant heat transfer coefficient is used for the hot fluid and the heat transfer coefficient for the cold fluid is determined according to the state of the fluid by linear interpolation from three heat transfer coefficients. The results demonstrate that small scale ORCs are well adapted to waste heat recovery with variable heat source flow rate and temperature.

Vaja [5] introduces an object oriented component library for advanced energy systems simulation. The study includes different modeling techiques for energy systems, the existing fluid models in different software environments, library for dynamic models of energy system components, and the application of those models in an energy system. The library of the components is built in the Simulink®. A dynamic model of an ORC system is also presented in the study.

Twomey [6] studies dynamic modeling and experimental verification of an ORC system. The system is constructed with ThermoPower and ThermoCycle, which are available in the Modelica environment. The simulation is made by Dymola simulation tool. The plate heat exchangers of the study are modeled in detail. Mass and energy dynamics are employed for the heat exchanger, different correlations for single-phase and two-phase flow are introduced. The simulation data are validated via real life experiment which conducted in the laboratory. According to the results the simulation outcomes are matched up with the experimental outcomes very closely.

Bracco *et al.* [7] introduce a laboratory prototype of an Organic Rankine Cycle. Main components of the system are a plate condenser, pump, electric boiler and a scroll expander. The working fluid is selected as r245fa. The presented ORC system achieves electric efficiency of 8% despite the conducted experiments did not undergo an optimization process. A dynamic model of the ORC is constructed with a commercial software for the modelization and analysis of single dimensional systems. Three simulation cases are constructed with different vapour generator outlet temperatures, which are the input temperatures for the ORC system. The dynamic model needs a calibration with the real life results, then it performs well by predicting the main system operating values.

Lee *et al.* [8] show transient responses of a 50 kW ORC system by altering the mass flow rate of the cooling water in the condenser. The refrigerant is selected as r245fa. The transient behaviour of the output power, condensing pressure and evaporation pressure is scoped and presented. According to the results there is strong inverse proportion between cooling fluids mass flow rate and the working fluids mass flow rate. At the time when the mass flow rate of the cooling water increased, there is no mass flow rate of the r245fa observed, and there is no power generation during that time.

Zhang *et al.* [9] study a numerical dynamic model of an 100 kW ORC system with a control model. The dynamic model is constructed by utilizing moving boundary methodology for the evaporator and the condenser. The dynamics of the system are introduced and linearized before they are put in a state space format. Later a multivariable control algorithm is designed and the simulations are performed. According to the results the system is able to produce the power demand satisfactorily, the control system performs well, even if there is disturbance in the system. Moreover, the introduced control algorithm is easy to implement in other power plants.

Colonna and van Putten [10,11] present dynamic model principles for steam power cycles in a two part work. In the first part [10], distinctions between dynamic model methodologies, modules, correlations and governing equations are presented, and the validation of a steam cycle simulation is discussed. SimECS, a simulator developed by Delft University that works according to modular, hierarchical and causal principles, is used as the simulator. In the second part [11], a small simple Rankine cycle system is simulated. The system configuration is based on the modules introduced in [10]. The Rankine cycle works as a biomass fired steam power plant. SimECS is used to simulate the transient response of the system when the rotational speed of the feed water pump undergoes a step increase, or when entering mass flow rate of exhaust gas undergoes a step or ramp change. The results reported are consistent but there is no validation with existing experimental data. On the other hand, the validation of the modules that are utilized in the Rankine cycle is achieved in [10] using available experimental data.

Li and Alleyne [12] establish a dynamic vapor compression cycle model as an extension of the recent study by McKinley and Alleyne [13], and perform start-up and shut-down operations. Their heat exchanger model is based on switching moving boundary model introduced by McKinley and Alleyne. They use void fraction data for switching criteria and introduce pseudo-state variables for accommodating transient dynamic states. The system is modeled under MATLAB® environment, and results indicate that start-up and shut-down operations are simulated successfully.

Casella *et al.* [14] present a steam cycle model and its optimization to achieve minimum start-up time. Optimization, simulation, and analyses are all conducted via an open source Modelica based platform. The limiting factor of the optimization problem is the stress caused by temperature difference between the body of the rotor and its outer surface. In the model, the steam turbine is discretized to gather the temperature distribution for stress calculation. A lumped temperature model is used for heat exchangers since only one temperature is measured for each side of the heat exchanger (hot and cold). Moreover, an algebraic model is used for the gas turbine model due to its short dynamic response compared with the overall system and to simplify the model.

Bamgbopa and Uzgoren [15] work on a quasi-dynamic model for an ORC with working fluid r245fa. It is called quasi-dynamic, since static models are employed for the pump and the turbine. Discrete models are used for the evaporator and the condenser; these components are considered critical since they are the principal media of heat transfer in and out of the ORC. To simplify the model, it is assumed that the main heat transfer mechanism in fluid flow is convection, that heat transfer is solely between the fluids with perfect insulation of the outer pipe, and that the flow in pipes is without viscous effects. An explicit scheme is used for solving the governing discrete equations. Momentum equation is neglected because the model excludes pressure drop. Gnielinski equation [2] is used for single phase heat transfer correlation, whereas in the two phase state multiple correlations are employed for comparison.

Espinosa *et al.* [16] investigate transient ORC modeling for waste heat recovery on a truck to study start-up and shut-down phases. A commercial fluid dynamic simulation tool is used to simulate the system. The results indicate that transient simulations are crucial for understanding the cycle's behavior in critical situations such as the start-up phase. Apart from simulation of transients, initial conditions and initialization of the cycle are also important for reaching desired steady state conditions.

Ziviani *et al.* [17] present a review of advances and challenges in the low grade thermal energy utilization as an energy source. The work claims that despite the progress in the last years, low temperature applications need to be improved in efficiency, since most effective systems are expected in the high temperature ranges. Most common and market-ready technology in the low temperature range is said to be the ORC, but the need for flexible and reliable simulation models for optimization is acknowledged.

Chowdhury *et al.* [18] develop a dynamic model for an ORC that operates in supercritical pressure. The necessity for a transient model instead of steady state model arises when the variations in heat input are considered. It is claimed that thermal inertia of the system is governed by the evaporator, which is modeled with the finite volume approach. The condenser is not modeled separately, and it is assumed to be able to cool down the fluid to the desired temperature. The pump and the turbine are modeled at steady state since their response is relatively fast.

Summing up, in past researches, different models are constructed to represent the transients of an ORC. Usually, the heat exchangers are responsible with the transient behaviour of the complete cycle, and, lumped models are likely to be constructed for the pump and the turbine. In most of the studies, commercial simulation tools are adopted, for example Modelica is a popular simulation environment for the ORC. However, previous studies lack some transients in simulations. First of all, almost all simulations go from one steady state to another by changing single input. An open loop simulation study is still needed for the ORC. Second, in some research, pressure is held constant in time, and the transient response is gathered from deviations in the heat input. Third, in the studies so far, the spatial distribution of the mass flow rate inside the heat

exchanger and it's effect on the transient model is not discussed. In the present study, an open loop and flexible ORC system is designed to carry out any change in any input in any time. The flexibility arises from the compatibility of working with component libraries. The simulation is constructed code-based in MATLAB environment, and numerical solution methodologies are presented. Moreover, the spatial distribution of mass flow rate inside the heat exchangers and its effect on the system's transients are introduced. To model transient ORC accurately, heat exchangers should be modeled in detail. The literature related to the modeling of heat exchangers will be mentioned in the following sections.

### 1.1.3. Modeling of Heat Exchangers

Governing most of the transients of the system makes dynamic modeling of the heat exchanger vital. Modeling of the heat exchanger becomes more complex when working fluid experiences phase change. For example, if evaporation or condensation is observed in the heat exchanger, the thermal state properties of the flow change dramatically which leads to introduction of various correlations between different phases. Moreover, the geometry impacts the heat transfer considerably. Hence, the numerical representation of the geometric properties is as important as the selection of proper heat transfer correlations. A robust model should be capable of estimating the heat transfer for any state of the working fluid even for the heat exchanger with a complex geometry. In the following sections the studies with different modelization approaches in the literature are summarized.

1.1.3.1. Analytical Approach. Ansari and Mortazavi [19] simulate a counterflow coaxial double pipe heat exchanger. The simulation method is based on the analytical solution of the energy balance equation based on the following three assumptions: (i) the wall conductance resistance is negligible in comparison with convective resistance, (ii) longitudinal heat conduction is neglected, (iii) heat transfer to outer environment is neglected. A discrete model is employed to calculate the temperature change for each cell. Comparison of experimental results with numerical results obtained by changing

the mass flow rate and the hot fluid inlet temperature shows that the model is capable of representing transient behavior correctly.

Al-Dawery *et al.* [20] discuss dynamic modeling and control of a plate heat exchanger, and their model is based on the solution of unsteady-state energy balance equation. The unsteady-state energy balance equation is linearized and Laplace transform is employed. Moreover, PID and fuzzy logic controllers are introduced. According to the results, fuzzy logic controller gives better results than conventional controllers.

Ebrahimzadeh *et al.* [21] model the dynamics of a plate heat exchanger. Runge-Kutta-Fehlberg method is employed for the solution of differential equations. The stated aim of building a device that eliminates the effects of transient perturbations seems to be achieved according to the experimental results shown. The numerical model predicts the exchanger behavior satisfactorily.

1.1.3.2. Moving Boundary Model. Jensen and Tummescheit [22] develop numerical model according to moving boundary formulation for the dynamic simulation of heat exchangers with two phase flow. In the model, flow enters the heat exchanger in liquid state and leaves the exchanger in vapor state. Governing equations are introduced for moving boundary models including subcooled, two phase and superheated regions. The influence of the void fraction on the system response is investigated. A new method for void fraction calculation is introduced, which is based on symbolic solution to the integral of the liquid fraction profile. The study claims that moving boundary method is very fast compared to discrete models and very robust to sudden changes in the boundary conditions.

1.1.3.3. Discrete Model. The famous study by Willatzen, Pettit and Ploug-Sorensen [23, 24] discusses dynamic modelling, simulation and control of heat exchangers. In the first part [23] they formulate numerically fast equations based on one dimensional flow equations. Mass and energy conservation and Newton's second law are the basics of theory. They mainly consider the heat transfer between wall material and working

fluid. In the second part [24] they perform simulation and control.

Valladares [25] studies on a triple concentric heat exchanger by means of transient analysis. Fluid mechanics governing equations and heat conduction theory in solids are employed in the study. Implicit formulation is utilized for numerical time integration. The study is superior to analytical approaches by considering transient effects, heat conduction and insulation, temperature dependent fluid properties and two phase flow conditions.

Xuan *et al.* [26] construct a generic dynamic model for heat exchangers based on energy and mass balance. The study is simple and clear in terms of application. Discretization method is utilized for numerical model. However heat transfer and pressure drop correlations are not specified in the study. The model also requires constant pressure level. According to results of the steady state simulation tool, the numerical model represents heat exchanger accurately.

Bracco *et al.* [27] present a numerical discretization method for dynamic simulation of a double-pipe heat exchanger. Discretized representation is employed for the numerical simulation model. Moreover, a PID controller is introduced to arrange hot fluid's outlet temperature by changing cold fluid's mass flow rate. In a simple geometry like double pipe system, the simulation acts like real system in the steady state or transient condition. For the heat exchangers with more complex geometries and different working fluids, it is expected that the discretized model will require finer mesh.

Zhao *et al.* [28] develop an evaporator model which uses r1234yf as the working fluid. Discretized model is employed and heat transfer rate is calculated by NTU-Effectiveness method. The model is able to represent the evaporator with low mean deviation 5.9% using Kandlikar's correlation for the two phase flow.

Different modelization techniques are discussed so far. The two popular numerical techniques are finite volumes discretization method and moving boundary method. On the other hand, some studies are based on the analytical solution of the governing

equations. The constructed model plays role in the energy system, that converts the heat input to the power output, hence, heat transfer rate calculation must be made accurately. Various heat transfer correlations for different flow properties are introduced in the literature so far. The summary of the studies is presented in the following section.

### 1.1.4. Heat Transfer Correlations for Heat Exchangers

Klimenko [29] studied a generalized correlation for two phase flow heat transfer. A reliable and comprehensive study for survey of correlations and experimenting their accuracies.

Admiraal and Bullard [30] study on variable conductance model, which is predicted to be more accurate than constant conductance model by taking change in flow state into account. The work is a comprehensive survey of two phase heat transfer correlations existed at that time. A comparison between the correlations is conducted and it is duscussed that which correlation works best at a certain condition. For examination of variable conductance model, the evaporator and the condenser are also modeled. As a result it is found that variable conductance model works better than constant conductance model as it is predicted.

Yan and Lin [31] examine the evaporation heat transfer and pressure drop in a vertical counter flow plate heat exchanger with a chevron angle of 60 degrees. The effects of quality, mass flow rate, heat flux and pressure of the system on the heat transfer and pressure drop are studied. In the study evaporation correlations for evaporators are also discussed.

Ayub [32] does a literature survey about single phase correlations for plate heat exchangers and presents some suggestions for two phase applications. Ayub also offers a two phase boiling and pressure drop correlations for flooded and direct expansion evaporators. Ayub's heat transfer correlation for two phase flow has a statistical error of 8%.

Palm and Claesson [33] present calculation methods for single and two phase flow in plate heat exchangers. The geometry of a plate heat exchanger is also introduced in the study. For the single phase flow, Muley and Manglik correlation and Martin's semi empirical equation are discussed. For the boiling flow, Cooper's pool boiling correlation is claimed to be the most appropriate correlation to be used for average predictions. According to the study, for the single phase correlations, the existing ones in open literature are in reasonable good accordance with experiments, however experimental verification for uncommon geometries are still needed.

Galeazzo *et al.* [34] study an Armfield FT-43 laboratory plate pasteurizer. A CFD model is employed to simulate the heat exchanger. The model contains approximately one million hexahedral elements. They use a commercial program GAMBIT® for mesh generation and another commercial program FLUENT® for solving the system with finite element method. Distilled water enters the system as both cold and hot fluid. A comparison is carried out between the experimental data and 1D plug flow model of Gut and Pinto (2003). Gut and Pinto's correlation is utilized, for calculating mean convective heat transfer coefficient. Numerical and experimental results fit well for one flow configuration. After having various configurations, the prediction from numerical model and data obtained from experiment have considerable differences. It is concluded that single heat transfer correlation, which depends on only one configuration, can't represent all configurations for a plate heat exchanger adaquetly. More accurate results are obtained with the 3D CFD model. In the both numerical models (3D CFD and plug flow model) heat load is calculated more than the experimental value however this is a expected behaviour, since the 3D CFD model does not take ambient heat losses into consideration. According to the results, in series flow arrangement CFD and plug-flow have same accuracy, while in parallel flow arrangement CFD works better. Moreover CFD has more detailed velocity and temperature distribution and it does not necessarily need to collect extensive experiment data to adjust model parameters.

Cascales *et al.* [35] present various heat transfer correlations for a plate heat exchanger. The investigation is made for single phase correlations and also for the boiling and the condensation heat transfer. For the single phase flow, Chisholm and

Wanniarachchi correlation [36], Kim correlation, Wanniarachchi correlation [37], Bogaert and Bolcs correlation, Muley correlation [37] and Martin correlation [38] are investigated. For boiling heat transfer, Yan and Lin correlation, Hsieh and Lin correlation, Han, Lee and Kim correlation, adopted Thonon correlation and asymptotic correlation are studied. For condensation, Yan, Lio and Lin correlation, Shah modified correlation, Kuo, Lie, Hsieh and Lin correlation, Han, Lee and Kim correlation and Thonon correlation are investigated. The results show that the correlations are in good agreement with experimented results.

Djordjevic and Kabelac [39] present experimental results on evaporation heat transfer on flow boiling of R134a and ammonia in a plate heat exchanger. One conclusion is that heat transfer increases with a high mass flow rate. For the low mass flow rates, heat transfer drops after vapour quality reaches about 0.5. It is mentioned that Steiner boiling correlation for vertical tubes can be adapted after some modifications for a valid prediction in plate heat exchanger theory.

Khan *et al.* [40] present a literature review to investigate the available heat transfer and pressure drop correlations for plate heat exchangers. The focus is mainly on evaporators. Heat transfer correlations for ammonia as well as other refrigerants such as r134a are introduced. Some of the included research are Yan and Lin (1999), Hsieh and Lin (2003) and Han *et al.* (2003). The effects of several operating parameters such as plate geometry and material still need to be quantified by experiments.

Abu-Khader [41] presents the recent studies on plate heat exchanger theory and applications. The study consists on reviews of research which have been conducted in the last decade. Heat transfer coefficient measurement, numerical and analytical models and two phase systems are studied in the presented research. The review does not include any correlations.

To sum up, various studies are conducted about dynamic modeling and simulation of an energy system, modeling of an heat exchanger and selecting proper heat transfer correlations. According to the studies, there are some distinctions while mod-

eling an energy system. Choosing moving boundary method or discretization method is a main distinction. Both methods have advantages and disadvantages. Moving boundary method works faster while discretization method is more flexible to the system configuration. Another distinction can be considered as choosing the integration technique. Some studies use commercial CFD programs such as FLUENT or SimECS, others come up with solution methods for the governing equations. This study will use discretized method and utilize MATLAB for solution of governing equations. On the other hand, in the most studies, mass flow rate of working fluid inside the heat exchanger is kept constant and the governing equations are solved according to this information. Moreover, system pressure is held constant in the ORC simulations. Especially at the starting up and shutting down phase, system pressure will overcome increase and decrease. This study aims to work with changing mass flow rate inside the heat exchanger and changing pressure level of the system. There exist more than one heat transfer correlation for single and two phase flow, they will be introduced in the following sections.

# 2. PHYSICAL MODEL AND GOVERNING EQUATIONS

The Organic Rankine Cycle (ORC) system considered in this study comprises an evaporator, a turbine, a condenser and a pump, connected via a pipe system conveying the fluid. The overview is presented in Figure 3.1. The dynamic simulation of the ORC requires the simulation of the fluid flow, considered irrotational and inviscid, with phase changes incurred by heat transfer. This flow is essentially one dimensional (1D), but here the relevant equations are first stated in their general form and then specialized for the problem at hand.

The flow considered herein is governed by three conservation laws: conservation of mass, of momentum, and of energy. These laws will be considered as applied to the control volume $\mathcal{V}$ shown in Figure 2.1.

## 2.1. Organic Rankine Cycle Components

### 2.1.1. Heat Exchangers

Heat exchangers are the most important components of ORCs. Since their dynamic response time is relatively long, they govern the system's transient action. A detailed model of the exchangers is therefore needed for the dynamic ORC model. Such a detailed model requires the geometry of the heat exchanger and the proper definition of the physical model equations.

2.1.1.1. Conservation of Mass. The conservation of mass requires that the material derivative of the mass $m$ enclosed in the control volume should be zero. This condition may be stated mathematically as

$$\frac{Dm}{Dt} = \int_{\mathcal{V}} \frac{\partial \rho}{\partial t} \, \mathrm{d}\mathcal{V} + \int_{\mathcal{S}} \rho \vec{v} \cdot \vec{n} \, \mathrm{d}\mathcal{S} = 0 \tag{2.1}$$

where $\rho$ denotes mass density at a point, $\mathcal{V}$ denotes the volume, $\mathcal{S}$ denotes the bounding surface area, $\vec{v}$ is the velocity vector at a point, $\vec{n}$ is the unit outward normal at that same point, and $\rho\vec{v}\cdot\vec{n}$ is the mass flux per unit surface area. The geometric variables are shown graphically in Figure 2.1a. Using the divergence theorem, Equation (2.1) may be recast in the conservative form:

$$\int_{\mathcal{V}} \left[\frac{\partial \rho}{\partial t} + \vec{\nabla}\cdot(\rho\vec{v})\right] \mathrm{d}\mathcal{V} = 0 \tag{2.2}$$

where $\vec{\nabla}$ is the vector differential operator; in rectangular cartesian coordinates it is given by the following expression, with $\vec{i}_x$, $\vec{i}_y$ and $\vec{i}_z$ denoting unit vectors along the $x$, $y$ and $z$ axes:

$$\vec{\nabla} = \vec{i}_x\frac{\partial}{\partial x} + \vec{i}_y\frac{\partial}{\partial y} + \vec{i}_z\frac{\partial}{\partial z} \tag{2.3}$$

If the flow is one dimensional (1-D) along the $x$ direction, Equation (2.2) simplifies to the following expression for the control volume shown in Figure 2.1b:

$$\int_{x}^{x+\Delta x} \left[\frac{\partial(\rho A)}{\partial t} + \frac{\partial(\rho A v)}{\partial x}\right] \mathrm{d}x = 0 \tag{2.4}$$

Here, $A$ is the constant cross sectional area of the pipe conveying the flow, and $v$ is the flow speed along $x$.

The mass flow rate across a cross section in 1-D flow is defined as

$$\dot{m} = \rho A v \tag{2.5}$$

such that with this definition, Equation (2.4) may be recast as:

$$\int_{x}^{x+\Delta x} \frac{\partial(\rho A)}{\partial t}\,\mathrm{d}x = -\int_{x}^{x+\Delta x} \frac{\partial \dot{m}}{\partial x}\,\mathrm{d}x \tag{2.6}$$

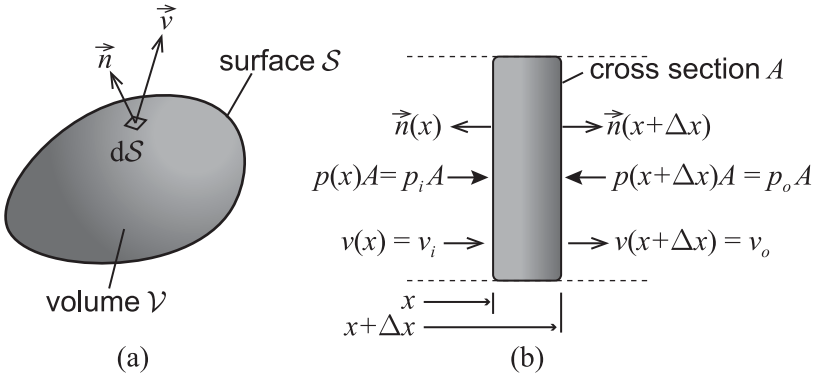


Figure 2.1. (a) A general control volume, (b) control volume for the one dimensional flow considered.

2.1.1.2. Conservation of Momentum. Conservation of momentum requires that the material derivative of linear momentum $\vec{L}$ be equal to the resultant $\vec{F}$ of the external forces. Taking into account the momentum flux $\rho\vec{v}(\vec{v}\cdot\vec{n})$ across the boundary, this condition may be stated as [5]:

$$\frac{D\vec{L}}{Dt} = \int_{\mathcal{V}} \frac{\partial(\rho\vec{v})}{\partial t}\,\mathrm{d}\mathcal{V} + \int_{\mathcal{S}} \rho\vec{v}(\vec{v}\cdot\vec{n})\,\mathrm{d}\mathcal{S} = \vec{F} \tag{2.7}$$

The resultant (vector sum) $\vec{F}$ includes surface (such as friction and pressure) and volumetric (such as gravity) forces. For the control volume of Figure 2.1b the flow is one dimensional along $x$ such that, using the definition of mass flow rate give in Equation (2.5) and the conservative form, Equation (2.7) simplifies to:

$$\int_x^{x+\Delta x} \frac{\partial \dot{m}}{\partial t}\,\mathrm{d}x + \int_x^{x+\Delta x} \frac{\partial(\dot{m}v)}{\partial x}\,\mathrm{d}x = F_x \tag{2.8}$$

where $F_x$ is the resultant force component along $x$, i.e. the flow direction.

Neglecting friction and gravity, the pressure $p$ (positive valued if compressive) is the only external effect such that Assuming the pressure distribution to be constant

over the cross section area $A$, one gets,

$$F_x = Ap(x) - Ap(x + \Delta x) = A(p_i - p_o) = -\frac{\partial(pA)}{\partial x}\Delta x \tag{2.9}$$

and the conservation of momentum requirement for the control volume of Figure 2.1b may be expressed as:

$$\int_x^{x+\Delta x} \frac{\partial \dot{m}}{\partial t}\,\mathrm{d}x + \int_x^{x+\Delta x} \frac{\partial(\dot{m}v)}{\partial x}\,\mathrm{d}x = -\frac{\partial(pA)}{\partial x}\Delta x \tag{2.10}$$

2.1.1.3. Conservation of Energy. Let $u$ denote the internal energy at a point per unit mass such that the total internal energy $U_{\mathcal{V}}$ for the control volume is given by:

$$U_{\mathcal{V}} = \int_{\mathcal{V}} \rho u\,\mathrm{d}\mathcal{V} \tag{2.11}$$

The rate of change of this internal energy will depend on mechanical and thermal inputs such that

$$\frac{DU_{\mathcal{V}}}{Dt} = \int_{\mathcal{V}} \frac{\partial(\rho u)}{\partial t}\,\mathrm{d}\mathcal{V} + \int_{\mathcal{S}} u\rho\vec{v}\cdot\vec{n}\,\mathrm{d}\mathcal{S} = \Pi + \Phi \tag{2.12}$$

where $u\rho\vec{v}\cdot\vec{n}$ is the internal energy flux per unit area, and $\Pi$ and $\Phi$ are the mechanical and thermal inputs. Energy dissipation and potential energy losses are neglected in our model and there is no energy generation within the fluid. Furthermore, the only external forces included are due to pressure. With these considerations, Equation (2.12) may be rewritten as

$$\int_{\mathcal{V}} \frac{\partial(\rho u)}{\partial t}\,\mathrm{d}\mathcal{V} + \int_{\mathcal{S}} \rho u(\vec{v}\cdot\vec{n})\,\mathrm{d}\mathcal{S} = \int_{\mathcal{S}} -p\vec{v}\cdot\vec{n}\,\mathrm{d}\mathcal{S} - \int_{\mathcal{S}} \vec{q}\cdot\vec{n}\,\mathrm{d}\mathcal{S} \tag{2.13}$$

where $\vec{q}$ is the heat outflow vector. Flow is one dimensional, yet the heat flux is longitudinal in the form of conduction and transversal in the form of heat transfer between fluids. The control surface can be considered in two parts: $\mathcal{S}_{//}$, which has its

outward normal vector parallel to the flow; and $\mathcal{S}_\perp$, which has its outward normal vector perpendicular to the flow direction. Heat transfer through conduction and convection takes place through $\mathcal{S}_{//}$. According to the Fourier model, the flow $\vec{q_c}$ of heat due to conduction is determined by $\vec{q_c} = -k\vec{\nabla}T$, with $k$ denoting conductivity and $T$ denoting the absolute temperature field. On the other hand, heat flow between cold and hot fluids is carried out through $\mathcal{S}_\perp$: heat transfer per unit area between hot and cold fluids is denoted by $\bar{q}$, and its calculation will be explained in following sections. With these definitions, the surface integral of heat outflow can be written in two components:

$$-\int_{\mathcal{S}} \vec{q}\cdot\vec{n}\,\mathrm{d}\mathcal{S} = -\int_{\mathcal{S}_{//}} (-k\vec{\nabla}T)\cdot\vec{n}\,\mathrm{d}\mathcal{S} + \int_{\mathcal{S}_\perp} \bar{q}\,\mathrm{d}\mathcal{S} \tag{2.14}$$

In simulating the exchanger and the condenser, pressure drop is expected to be small, such that the mechanical work contributions are considered as negligible:

$$\int_{\mathcal{S}} -p\vec{v}\cdot\vec{n}\,\mathrm{d}\mathcal{S} \approx 0 \tag{2.15}$$

In addition, $\Delta u = c\Delta T$, where $c$ is the specific heat. Considering the particular 1-D flow represented by the control volume in Figure 2.1b with the aforementioned simplifications, and also keeping in mind that $\dot{m} = \rho A v$, the conservation of energy requirement may be stated as follows:

$$\int_x^{x+\Delta x} \frac{\partial(\rho A c T)}{\partial t}\,\mathrm{d}x + \int_{\mathcal{S}} u\rho\vec{v}\cdot\vec{n}\,\mathrm{d}\mathcal{S} = -\int_{\mathcal{S}_{//}} (-k\vec{\nabla}T)\cdot\vec{n}\,\mathrm{d}\mathcal{S} + \int_{\mathcal{S}_\perp} \bar{q}\,\mathrm{d}\mathcal{S} \tag{2.16}$$

Using the divergence theorem leads to

$$\int_{\mathcal{S}} u\rho\vec{v}\cdot\vec{n}\,\mathrm{d}\mathcal{S} = \int_{\mathcal{V}} \vec{\nabla}\cdot(cT\rho\vec{v})\,\mathrm{d}\mathcal{V} = \int_x^{x+\Delta x} \frac{\partial(\dot{m}cT)}{\partial x}\,\mathrm{d}x \tag{2.17}$$

and

$$\int_{\mathcal{S}} (-k\vec{\nabla}T)\cdot\vec{n}\,\mathrm{d}\mathcal{S} = \int_{\mathcal{V}} -k\nabla^2 T\,\mathrm{d}\mathcal{V} = \int_x^{x+\Delta x} -kA\frac{\partial^2 T}{\partial x^2}\,\mathrm{d}x \tag{2.18}$$

where $\nabla^2 = \vec{\nabla} \cdot \vec{\nabla}$ is the Laplace operator, given by $\nabla^2 = \frac{\partial^2}{\partial x^2} + \frac{\partial^2}{\partial y^2} + \frac{\partial^2}{\partial z^2}$ in rectangular coordinates. The term representing heat transfer between fluids simplifies in 1-D to

$$\int_{\mathcal{S}_\perp} \bar{q} \, \mathrm{d}\mathcal{S} = \int_x^{x+\Delta x} \bar{q} B \, \mathrm{d}x \tag{2.19}$$

where $B$ is the perimeter at x through which the heat transfer occurs. Finally the conservation of energy requirement may be stated as follows:

$$\int_x^{x+\Delta x} \frac{\partial(\rho A c T)}{\partial t} \, \mathrm{d}x = -\int_x^{x+\Delta x} \frac{\partial(\dot{m} c T)}{\partial x} \, \mathrm{d}x + \int_x^{x+\Delta x} kA \frac{\partial^2 T}{\partial x^2} \, \mathrm{d}x + \int_x^{x+\Delta x} \bar{q} B \, \mathrm{d}x \tag{2.20}$$

By definition, enthalpy $H$ is a measure of energy and its relation with internal energy can be expressed as $H = U + p\mathcal{V}$ [42]. Specific enthalpy, $h$, is a state variable and it is defined as enthalpy per unit mass. For constant pressure and constant density the change in specific enthalpy is equal to the change in the specific energy, i.e. $\Delta h = \Delta u$. Recalling that for constant pressure $\Delta u = c\Delta T$ , the energy conservation equation can be recast into enthalpy dynamics:

$$\int_x^{x+\Delta x} \frac{\partial(\rho A h)}{\partial t} \, \mathrm{d}x = -\int_x^{x+\Delta x} \frac{\partial(\dot{m} h)}{\partial x} \, \mathrm{d}x + \int_x^{x+\Delta x} kA \frac{\partial^2 T}{\partial x^2} \, \mathrm{d}x + \int_x^{x+\Delta x} \bar{q} B \, \mathrm{d}x \tag{2.21}$$

2.1.1.4. Heat Transfer Equations. The heat exchangers that operate in an ORC system are the evaporator, the condenser, and the chiller. These components are critical for transient analysis of the cycle. The heat transfer rate of the heat exhanger is an important parameter for the dynamic system, since the heat transfer rate has direct bearing on the time period for reaching steady state operating conditions. Heat transfer rate can be predicted by conducting an analysis by scoping the thermodynamic state characteristics of the fluid, and the geometry and operating conditions of the heat exchanger. In this context some quantities such as heat transfer surface area, inlet and outlet temperatures of fluids, and the overall heat transfer coefficient should be defined. The log mean temperature difference (LMTD) method can be used to perform such analyses and estimate the heat transfer rate. Apart from the inlet temperatures of

both fluids, the LMTD method also requires the outlet temperature of one of the fluids in order to complete necessary calculations based on energy balance. Unfortunately, when a dynamic model is taken into account, one does not have any information about outlet temperatures. An iterative computation initiated with an initial estimate of the outlet temperature is necessary for the LMTD method when a transient heat exchanger analysis is aimed. It therefore may be preferable to use another approach called the effectiveness–number of transfer units ($\varepsilon$-NTU) method. The $\varepsilon$-NTU method is based on calculating a maximum heat transfer capacity based on inlet temperatures and heat capacities of the fluids. Then, utilizing correlations appropriate to the flow and heat exchanger characteristics (heat exchanger geometry, parallel, cross or counter flow), an effectiveness value is found. In those correlations dimensionless parameters are used such as heat capacity ratio $C_r$ [43] defined as

$$C_r = \frac{C_{min}}{C_{max}} \tag{2.22}$$

In this expression, $C$ denotes the heat capacity of fluid and it is calculated by

$$C = \dot{m}c \tag{2.23}$$

$C_{min} = \min(C_C, C_H)$, $C_{max} \max(C_C, C_H)$, and $C_C$ and $C_H$ denote the heat capacity for the cold and the hot fluids, respectively. The number of transfer units $NTU$ is given by ( [43])

$$NTU = \frac{\theta A_{\mathcal{S}\perp}}{C_{min}} \tag{2.24}$$

where $\theta$ is overall heat transfer coefficient, which will be explained following sections. $A_{\mathcal{S}\perp}$ is the heat transfer area, i.e. the area of the surface through which heat transfer occurs $\mathcal{S}_\perp$. The last dimensionless parameter $\varepsilon$ is called effectiveness and it is defined by ( [43])

$$\varepsilon = \frac{q}{q_{max}} \tag{2.25}$$

where $q_{max}$ is the maximum heat transfer capacity calculated from $q_{max} = C_{min}\Delta T$, with $\Delta T$ denoting the difference between the inlet temperatures of the hot and cold fluids. The effectiveness is essentially used to determine $q$ from Equation (2.25): it is given by $\varepsilon = \varepsilon(NTU, C_r)$, and $\varepsilon(NTU, C_r)$ is calculated based on the fact that the temperature differences at the inlet and outlet may be redefined in terms of the heat capacity ratio of the fluids, and the ratio of the overall heat transfer coefficient to the heat capacity of the cold fluid [37]. Since $\varepsilon$-NTU is more compatible with the dynamic model, $\varepsilon$-NTU is employed for the heat transfer rate estimation.

2.1.1.5. $\varepsilon$-NTU method. The $\varepsilon$-NTU method is used for calculating the heat transfer rate between fluids inside the heat exchanger. To begin with, the flow must be categorized as laminar or turbulent according to the Reynolds number $Re$ defined as ( [43])

$$Re = \frac{\rho v D_{hyd}}{\mu} \tag{2.26}$$

where $\rho$ is density, $v$ is mean velocity of the flow, $D_{hyd}$ is hydraulic diameter, and $\mu$ means dynamic viscosity of the fluid. If $Re$ <2000, the flow is laminar; else, it is turbulent. In general, the velocity profile of the flow is not constant through the cross section; due to frictional effects, the speed of the flow at the boundary is less than the flow speed the center of the cross section. At locations where flow speed is low, heat transfer is largely governed by conduction. On the contrary case, at the center of the cross section, heat transfer is governed by the convection rather than the conduction. The Nusselt number $Nu$ is a dimensionless parameter, defined as the ratio of convection to the conduction heat transfer. $Nu$ is defined as ( [43])

$$Nu = \frac{h\, D_{hyd}}{k} \tag{2.27}$$

where $I$ is the convective heat transfer coefficient and $k$ is conductive heat transfer coefficient. There exist various correlations for the Nusselt number in the literature: for the single phase flow, correlations for plate heat exchangers are provided in [37]

and [44]. In these correlations certain geometric properties of the plate heat exchanger must be known; for example, the chevron angle of the plate is selected as $\beta = 30$ degrees in this study. The chevron angle and other geometric properties will be defined in the geometric equations section. The following correlation for the Nusselt number, initially proposed by Tovazhnyanski et al. [45], is introduced by Kakac and Liu [37]:

$$Nu = 0.051e^{[0.64tan\beta]}Re^{0.73}Pr^{0.43}(\frac{Pr}{Pr_w})^{0.25} \tag{2.28}$$

where $Pr$ is the Prandtl number and $Pr_w$ is the Prandtl number of at wall conditions; $\beta$ denotes the chevron angle of the exchanger. Another correlation for the Nusselt number, originally proposed by Martin [38], is introduced by Shah and Sekulic [44]:

$$Nu = 0.205Pr^{1/3}\left(\frac{\mu}{\mu_w}\right)^{1/6}(f \cdot Re^2 sin2\beta)^{0.374} \tag{2.29}$$

where $\mu$ is dynamic viscosity, $\mu_w$ is the dynamic viscosity at wall conditions, and $\beta$ is the chevron angle of the plate heat exchanger. $f$ is the Fanning friction factor for which Martin [38] proposes the following expression:

$$\frac{1}{\sqrt{f}} = \frac{\cos\beta}{(0.045\tan\beta + 0.09\sin\beta + f_0/\cos\beta)^{1/2}} + \frac{1-\cos\beta}{\sqrt{3.8f_1}} \tag{2.30}$$

The parameters $f_0$ and $f_1$ are defined as:

$$f_0 = \begin{cases} 16/Re & \text{for } Re < 2000 \\ (1.56\ln Re - 3.0)^{-2} & \text{for } Re \geq 2000 \end{cases} \tag{2.31}$$

$$f_1 = \begin{cases} (149.25/Re) + 0.9625 & \text{for } Re < 2000 \\ 9.75/Re^{0.289} & \text{for } Re \geq 2000 \end{cases} \tag{2.32}$$

The heat transfer coefficient for convection is then given by:

$$I = \frac{kNu}{D_{hyd}} \tag{2.33}$$

Another correlation for Nusselt number, proposed originally by Chisholm and Wanniarachchi [36], is also presented in [37]. The correlation is valid for chevron angles between 30 and 80 degrees and for Reynolds number between 1000 and 4000:

$$Nu = 0.72 Re^{0.59} Pr^{0.4} \phi^{0.41} \left(\frac{\beta}{30}\right)^{0.66} \tag{2.34}$$

where $\phi$ is the ratio of the actual effective area (specified by the manufacturer) to the projected plate area, calculated as follows:

$$\phi = \frac{A_{tr}}{\Lambda_p \times \Lambda_w} \tag{2.35}$$

where $\Lambda_p = l_v - D_p$,and $\Lambda_w = l_h + D_p$, $l_v$ is vertical port distance, $l_h$ is horizontal port distance, and $D_p$ is port diameter as it is presented in Figure 2.3. These variables will be further explained in a latter section. For the two phase flow there also exists more than one correlation in the literature. Gungor and Winterton [46] correlation and Shah [47] correlation are discussed in [37]. Gungor and Winterton correlation is given by:

$$I_2 = a_1 I_{lq} + a_2 I_{pool} \tag{2.36}$$

$I_{lq}$ is all liquid convection heat transfer coefficient. It is calculated from the Dittus-Boelter equation ( [37]) as:

$$I_{lq} = 0.023 \left[\frac{G(1-\kappa)D_{hyd}}{\mu_{lq}}\right]^{0.8} Pr^{0.4} \frac{k_{lq}}{D_{hyd}} \tag{2.37}$$

where $G$ equals to $\rho v$, $k_{lq}$ means conductivity of the fluid in the liquid state, $\kappa$ represents quality of the flow, and $\mu_{lq}$ means dynamic viscosity of the fluid in the liquid state.

The coefficient $a_1$ in Equation (2.36) is calculated from

$$a_1 = 1 + 2.4 \times 10^4 \mathfrak{b}_o^{1.16} + 1.37 \left(\frac{1}{X_{tt}}\right)^{0.86} \tag{2.38}$$

where the boiling number $\mathfrak{b}_o$ is defined as:

$$\mathfrak{b}_o = \frac{q''}{GY} \tag{2.39}$$

In this expression, $Y$ is the latent heat of working fluid, $q''$ is the heat flux to the fluid and $X_{tt}$ is the Martinelli parameter to be calculated as follows:

$$X_{tt} = \left(\frac{1-\kappa}{\kappa}\right)^{0.9} \left(\frac{\rho_{gs}}{\rho_{lq}}\right)^{0.5} \left(\frac{\mu_{lq}}{\mu_{gs}}\right)^{0.1} \tag{2.40}$$

Where $\rho_{gs}$ is the density of the fluid in the gas state, $\rho_{lq}$ defines the density in the liquid state, $\mu_{lq}$ represents the dynamic viscosity of the fluid in the liquid state, and $\mu_{gs}$ means the dynamic viscosity of the fluid in the gas state. The quality of the fluid is represented by $\kappa$. The coefficient $a_2$ in Equation (2.36) is given by:

$$a_2 = \frac{1}{1 + 1.15 \times 10^{-6} a_1^2 Re_{lq}^{1.17}} \tag{2.41}$$

where $Re_{lq}$ is calculated from

$$Re_{lq} = \frac{G(1-\kappa)D_{hyd}}{\mu_{lq}} \tag{2.42}$$

Then, $I_{pool}$ from the equation 2.36 is defined as:

$$I_{pool} = 55 Pr^{0.12} (-log_{10} Pr)^{-0.55} M^{-0.5} (q'')^{0.67} \tag{2.43}$$

where $M$ is the molecular weight of the working fluid.

Shah correlation for two phase heat transfer coefficient $I_2$ is presented in [37] as follows:

$$I_2 = \Psi I_{lq} \tag{2.44}$$

Here, $I_{lq}$ is all liquid heat transfer correlation and it is obtained by the Dittus - Boelter given in Equation (2.37). For the vertically oriented heat exchangers, since all heat exchanger surface is wet, the Froude number is not calculated. Apart from the Froude number, one still needs to calculate two dimensionless numbers: the convection number $\mathfrak{c}_o$ and the boiling number $\mathfrak{b}_o$. Boiling number is obtained via Equation (2.39). Convection number is calculated from ( [37]):

$$\mathfrak{c}_o = \left(\frac{1}{\kappa} - 1\right)^{0.8} \left(\frac{\rho_{gs}}{\rho_{lq}}\right)^{0.5} \tag{2.45}$$

Where $\kappa$ stands for the quality of the liquid. For the vertical flow, a new term $N_s$ is introduced as $N_s = \mathfrak{c}_o$.

$$\Psi_{cb} = \frac{1.8}{N_s^{0.8}} \tag{2.46}$$

There are three possible cases according to the value of the $N_s$, if $N_s > 1$:

$$\Psi_{nb} = 230\mathfrak{b}_o^{0.5} \tag{2.47}$$

for $\mathfrak{b}_o > 0.3 \times 10^{-4}$; else,

$$\Psi_{nb} = 1 + 46\mathfrak{b}_o^{0.5} \tag{2.48}$$

so that $\Psi$ equals to larger of $\Psi_{nb}$ and $\Psi_{cb}$. For $N_s < 1$, $\Psi_{bs}$ is calculated instead of $\Psi_{nb}$. If $N_s > 0.1$:

$$\Psi_{bs} = g_1 \mathfrak{b}_o^{0.5} e^{2.74 N_s^{-0.1}} \tag{2.49}$$

else if $N_s < 0.1$

$$\Psi_{bs} = g_1 \mathfrak{b}_o^{0.5} e^{2.47 N_s^{-0.15}} \tag{2.50}$$

and $\Psi$ equals to larger of $\Psi_{bs}$ and $\Psi_{cb}$. $g_1$ in Equations (2.49) and (2.50) is 14.7 if $\mathfrak{b}_o \geq 11 \times 10^{-4}$; else, $g_1 = 15.43$.

Once $I$ is calculated, the overall heat transfer coefficient $\theta$ is calculated from (neglecting wall conduction resistance, [43])

$$\frac{1}{\theta A_{\mathcal{S}\perp}} = \frac{1}{(I A_{\mathcal{S}\perp})_H} + \frac{1}{(I A_{\mathcal{S}\perp})_C} \tag{2.51}$$

As mentioned before, effectiveness $\varepsilon$ will be calculated from correlations. Recalling Equation (2.22), if heat capacities of both fluids are the same, then $C_r = 1$ ( [43]) and

$$\varepsilon = \frac{NTU}{1 + NTU} \tag{2.52}$$

If one of the fluids undergoes a phase change, then $C_r = 0$. The reason for heat capacity ratio to be zero is that the phase changing fluid's temperature is constant during the phase change, hence it's heat capacity is assumed to be infinity. In that case, effectiveness is defined for all kinds of heat exchangers as follows ( [43]):

$$\varepsilon = 1 - e^{(-NTU)} \tag{2.53}$$

For other $C_r$ values such that $0 < C_r < 1$ for single pass counterflow heat exchangers, effectiveness is found by

$$\varepsilon = \frac{1 - e^{-NTU(1-C_r)}}{1 - C_r e^{-NTU(1-C_r)}} \tag{2.54}$$

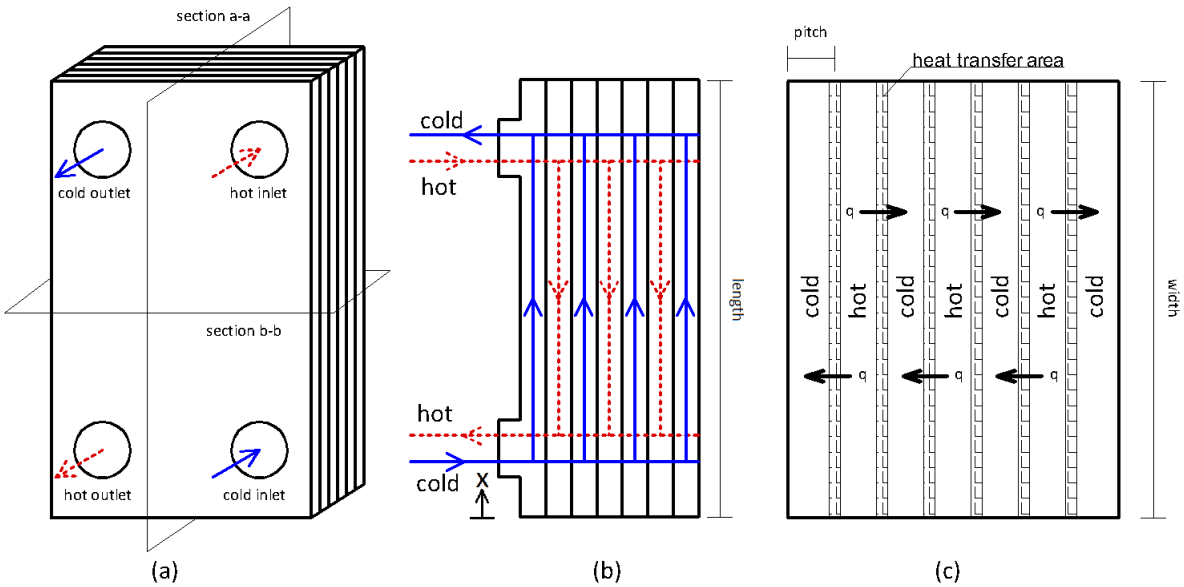


Figure 2.2. Geometry of the plate heat exchanger: (a) 3-D view, (b) Section a-a, (c) Section b-b

Then the heat transfer $q$ is obtained from Equation (2.25) as

$$q = \varepsilon q_{max} \tag{2.55}$$

2.1.1.6. Geometric equations:. The geometric properties of the heat exchangers are as important as the flow dynamics and heat transfer rate correlations. Counterflow single pass plate type heat exchangers are used inside the ORC system. Figure 2.2 shows the sections and a general 3-D view of the heat exchanger. The critical dimensions of the heat exchanger marked on Figure 2.2 are the length, the width, and the pitch. The width and the pitch affect the cross sectional area of flow and the heat transfer area.

In the exchanger there are $N_C$ number of cold fluid flow channels, and $N_H$ number of hot fluid flow channels. Length is the dimension along flow direction (denoted as $x$) and it is divided into infinitesimal length elements. The reason of the discretization is the expected phase change. The expected phase change will have major effect on the fluid properties, therefore one needs to discretize the heat exchanger to locate and formulate the subcooled, the two phase and the superheated regions. There are various

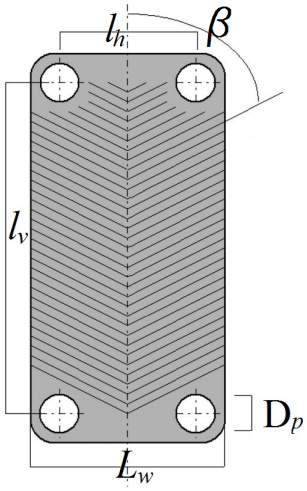


Figure 2.3. Geometry of a plate heat exchanger plate

ways to handle phase change phenomena, among which the moving boundary method and the finite volume method have found widespread popularity. In this study, the finite volumes method is selected. The heat exchanger is divided into finite volumes along the flow direction. The geometric properties of importance are the flow areas ($A_C$ and $A_H$) and the flow perimeters ($B_C$ and $B_H$) of the cold and hot fluids. These quantities are calculated using the following formulas:

$$A_C = L_w \cdot L_p \cdot N_C \tag{2.56}$$

$$A_H = L_w \cdot L_p \cdot N_H \tag{2.57}$$

$$B_C = 2N_C(L_p + L_w) \tag{2.58}$$

$$B_H = 2N_H(L_p + L_w) \tag{2.59}$$

In these expressions, $L_w$ is width of the plates and $L_p$ is the pitch distance between plates. An illustration of the heat exchanger plates is given in Figure 2.3.

The heat transfer area $A_{tr}$ is given by

$$A_{tr} = 2\frac{A_{pl}}{N_{subcells}} min(N_C, N_H) \tag{2.60}$$

Where the term $N_{subcells}$ denotes the number of discretization elements along the flow direction. The hydraulic diameter, $D_{hyd}$, is required for calculating the Reynolds number and also for heat transfer correlations. A formulation of hydraulic diameter for plate heat exchangers is given as ( [37])

$$D_{hyd} = \frac{2b}{\phi} \tag{2.61}$$

where $b = L_p - t_p$ and $\phi$ is calculated from equation 2.35.

### 2.1.2. Expander

An expander or a turbine expander is a component which extracts work from pressurized gas through expansion. In the numerical model, this component is modeled in its steady state operating conditions since expander's response time is relatively short in comparison with the response time of the heat exchanger. The extracted work is produced from the inlet and outlet enthalpy difference of the working fluid (in our case, r134a). Theoretically, the gas is assumed to be in its saturation enthalpy when leaving the expander. Depending on the design of the expander, unwanted liquifaction can be observed or some gas may leave the expander in it's superheated state. The latter situation points to poor efficiency of the expander design. The inlet enthalpy $h_1$ equals to outlet enthalpy of the evaporator. Expected outlet pressure, $p_o$ is pre-defined and it is less than inlet pressure. The work output is calculated as:

$$\dot{W} = \dot{m}(h_1 - h_2) \tag{2.62}$$

where the mass flow rate $\dot{m}$ equals to the outlet mass flow rate of the evaporator. The $h_2$ is the enthalpy of the working fluid at the expander outlet. It is calculated by:

$$\eta = \frac{h_1 - h_2}{h_1 - h_{2s}} \tag{2.63}$$

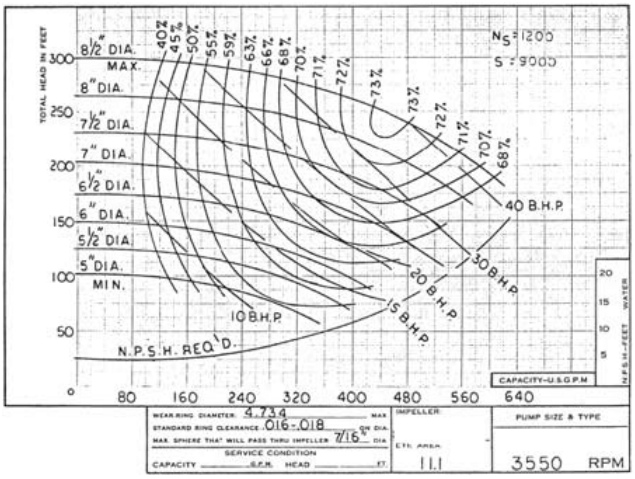


Figure 2.4. Typical published pump efficiency curve example

where $\eta$ denotes the efficiency of the expander and it is a pre-defined parameter (in our case, $\eta = 0.80$). The $h_{2s}$ is the enthalpy resulting isentropic expansion of for the fluid at the outlet pressure of the expander. In the numerical model the outlet enthalpy and mass flow rate are boundary values for the condenser.

### 2.1.3. Pump

In an ORC system, the pump is responsible for maintaining the flow. With its short response time, the pump is numerically modeled also in its steady state operating condition. A pump has three variables, which are related to each other by an efficiency curve. For a centrifugal pump, those three variables are the pressure head, the mass flow rate, and the rounds per minute (rpm) of the pump. The pump must supply essentially the existing pressure difference at the inlet and the outlet of the pump. Moreover, it should supply sufficient pressure to beat the internal pressure of the evaporator and maintain the flow. Based on these considerations, the desired rpm is selected depending on the pressure head difference and the desired mass flow rate. In the numerical model the outlet pressure and the outlet mass flow rate of the pump are boundary values for the evaporator. In Figure 2.4, an example of pump efficiency curve is presented.

### 2.1.4. ORC Governing Equations

The governing equations of entire cycle is calculated in previous sections and they will be presented in their final form in this section. The following governing equations for the heat exchangers are obtained by removing the integrals from corresponding equations:

- From mass conservation (2.6):

$$\frac{\partial(\rho A)}{\partial t} = -\frac{\partial \dot{m}}{\partial x} \tag{2.64}$$

- From momentum conservation (2.10):

$$\frac{\partial \dot{m}}{\partial t} + \frac{\partial(\dot{m}v)}{\partial x} = -\frac{\partial(pA)}{\partial x} \tag{2.65}$$

- From energy conservation (2.21):

$$\frac{\partial(\rho A h)}{\partial t} = -\frac{\partial(\dot{m}h)}{\partial x} + kA\frac{\partial^2 T}{\partial x^2} + q \tag{2.66}$$

The governing equation of the expander is as follows:

$$\dot{W} = \eta \dot{m}(h_1 - h_{2s}) \tag{2.67}$$

where subscript '1' stands for inlet and subscript '2s' stands for outlet isentropic enthalpy of the expander.

## 2.2. Steady State Equations

To operate in the steady state condition means that operating system has reached a balance and it will continue to keep that balance unless there is a perturbation. In mathematical terms, when the terms pertaining to the time rate of change are set to zero, the remaining terms will lead to the steady state solution. The steady state solution of the heat exchangers will help to rate the accuracy of the dynamic model, since the convergence to the steady state solution is expected when sufficient time is given to the dynamic simulation. Since mass and density values are time invariant in the steady state (which implies that mass flow rate is constant everywhere), only the energy balance equation will be taken into account for the solution of the system. Then the density values are function of enthalpy and pressure. Recalling the energy dynamics governing equation (2.66) and setting the time derivatives to zero one obtains:

$$0 = -\frac{\partial(\dot{m}h)}{\partial x} + kA\frac{\partial^2 T}{\partial x^2} + q \tag{2.68}$$

Since the conduction is assumed to be negligible, it can be left out, leading to:

$$0 = -\frac{\partial(\dot{m}h)}{\partial x} + q \tag{2.69}$$

The steady state equation (2.67) of the expander is valid and can be employed with steady state equation of the heat exchangers.

## 2.3. Selection of the State Variables

The dynamic model needs state variables, which are solved by governing equations, and, which define time dependent state of the system. Two alternatives exist when selecting the state variables. In the first one, model is based solely on the enthalpy dynamics. The thermodynamic state of the fluid can easily be defined by coupling specific enthalpy and pressure information. In the second one, it is possible to use temperature dynamics for constructing the model. However, temperature and

pressure values are useful to define thermodynamic state of the fluid only when it is in single phase. For the two-phase zone, a new state variable called 'quality', $\kappa$, is introduced. The quality denotes the ratio of the vapour mass to the total mass of the fluid. Moreover, specific enthalpy must be introduced to represent the transport of the energy. Thus, for simplicity, specific enthalpy, $h$, is a popular state variable for representing a energy system.

Based on the equation (2.66), the energy dynamics of the system is expressed with the specific enthalpy. Combining specific enthalpy value with a second state value (i.e. pressure), the other thermal state properties of the fluid can be determined. If the fluid is in the two-phase, the quality of the fluid is determined by specific enthalpy and pressure, or specific enthalpy and temperature. When the quality is 0, it denotes pure completely liquid state, and, when it is 1, it indicates the completely gas state, and the intervalues denote coexistence by mass ratio.

Subsequent to derivation the governing equations of an ORC system, selection of proper state variables, defining geometric definitions and properties of plate heat exchangers, and determining heat transfer correlations, the time dependent solutions to the presented governing equations should be computed to form the complete cycle. The discretization of the equations and utilization of numerical computing method are essential for the computation, the details to be discussed in the following section.

# 3. DISCRETIZATION AND NUMERICAL MODEL

Governing equations, heat transfer correlations and the geometric parameters of the plate heat exchanger are introduced so far. In this chapter, the governing equations of the dynamic model are solved to obtain the model's behavior. The numerical solutions are carried out by the finite volumes method. Steady state response and transient dynamics will be both addressed in the next sections.

## 3.1. Overview of the ORC

Following illustration, Figure 3.1 presents the simple Organic Rankine Cycle and components. The cycle is constructed in accordance with the one in the Bogazici University BURET Laboratory. The initialization of the system and a brief explanation of the loop will be discussed as follows.

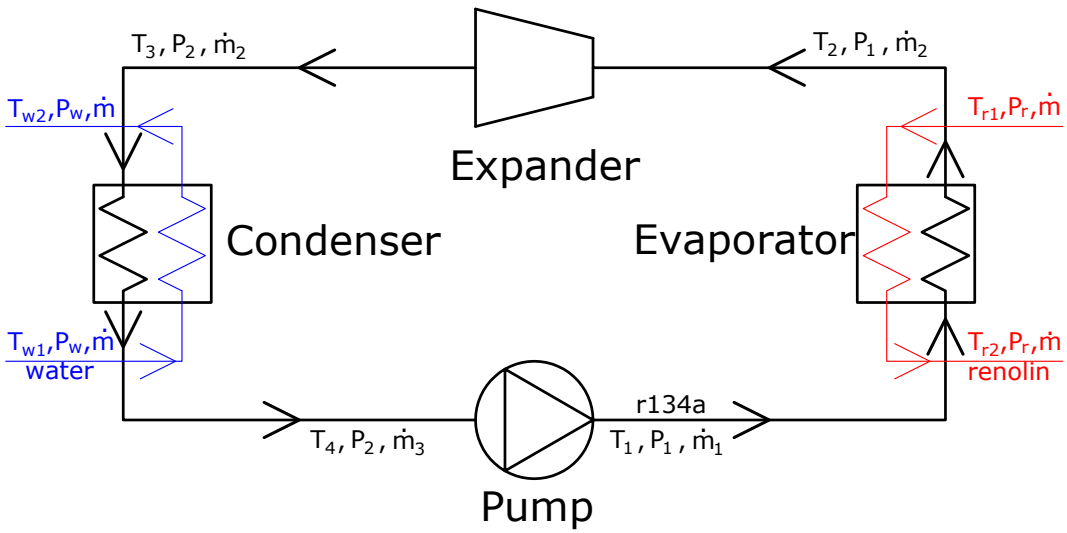


Figure 3.1. ORC overview and boundary values

### 3.1.1. Initialization

'Initialization' is the first step of a numerical dynamic simulation, in which required states of the cycle are calculated when $t = 0$. The initialization of the system is based on the assumption that when $t = 0$, the flow exists at uniform temperature everywhere in the cycle. The heat transfer only begins when the simulation runs. In other words, $T_2$, $T_3$, $T_4$ are equal to $T_1$ when $t = 0$. In addition $T_{r2} = T_{r1}$, and $T_{w2} = T_{w1}$ when the simulation begins. The cycle's starting point is the outlet of the pump, where $P_1$, $\dot{m}_1$ is defined by the pump. $T_1$ is usually chosen as the room temperature. The initialization involves determining density distribution inside the evaporator and the condenser, enthalpy distribution inside the evaporator and the condenser, and calculation of the enclosed mass by the evaporator and the condenser. The calculations mentioned above are made for the evaporator based on the values of temperature ($T_1$) and pressure ($P_1$). For the condenser, initialization is set based on $T_1$ and $P_2$ values. Since the pump and the expander are modeled in the steady state condition, $P_2$ should be defined before the simulation begins. State initializations of renolin and water are conducted based on 'renolin temperature 1', $T_{r1}$, 'renolin pressure', $P_r$, 'water temperature 1', $T_{w1}$, and 'water pressure', $P_w$. The invariants of the system are $P_r$, $\dot{m}$ of renolin and $P_w$. Every other terms, which are shown in Figure 3.1, are variables depending on the time.

### 3.1.2. The loop and boundary values in the cycle

As the simulation begins, heat transfer occurs in the heat exchangers, and therefore, different temperatures are measured in different locations of the cycle. Following inequalities show up $T_1 \neq T_2 \neq T_3 \neq T_4$, $T_{r2} \neq T_{r1}$, and $T_{w2} \neq T_{w1}$. Consequtively, values of the enthalpy and the density also change in different locations of the cycle. The enclosed mass by the heat exchangers deviate dramatically when working fluid changes its phase due to the heat transfer. Hence, the equality of $\dot{m}_1 = \dot{m}_2 = \dot{m}_3$ is broken until a steady state operating condition is reached. The mass flow rate of the working fluid (r134a) become a function of time and space, $\dot{m}_{1,2,3} = \dot{m}(t, x)$. The hot and cold fluids of the cycle, renolin and water respectively, do not encounter phase

change, and, their mass flow rates are assumed to be constant along the heat exchangers. The mass flow rate of the renolin is always constant as mentioned above. The mass flow rate of the water is controlled by the valve in the real system, therefore, it is introduced as a function of time solely, $\dot{m}_w = \dot{m}_w(t)$. The loop begins with the pump, $P_1$ and $\dot{m}_1$ are provided by the pump for any time in the simulation. $T_1$, $P_1$, $\dot{m}_1$, $T_{r1}$, $P_r$, $\dot{m}_r$ are the boundary values of the evaporator. $T_2$, $T_{r2}$, and $\dot{m}_2$ are the outcomes of the evaporator. The boundary values of the expander are $T_2$, $P_1$, $P_2$, and $\dot{m}_2$. $T_3$ is defined by the expander and becomes boundary value of the condenser along with $T_{w1}$, $P_w$ , $\dot{m}_w$, $\dot{m}_2$ and $P_2$. The outputs of the condenser are $T_4$, $T_{w2}$ and $\dot{m}_3$. To close the loop, $T_1$ is set equal to $T_4$. During the transient simulation $\dot{m}_1 \neq \dot{m}_3$, therefore change in the mass flow rate is expected in the pump, however in the real system, a tank is installed before the pump to overcome this variation. Hence, the mass dynamics are not introduced for the pump.

## 3.2. Discrete Steady State Equations

The steady state governing energy equation (2.69) is presented in the previous chapter. The discretized version of the equation is as follows:

$$h_i = h_{i-1} + \frac{q_{i-1}}{\dot{m}} \tag{3.1}$$

The enthalpies of the fluids at the entrance of the heat exchanger is known. The heat exchanger is counterflow, therefore enthalpy outlets of both fluids cannot be solved along with flow direction (i.e one of the fluids' outlet enthalpy value at the $(i+1)^{th}$ cell changes the heat transfer rate of other fluid at the $i^{th}$ subcell). A back and forth iteration is therefore required for obtaining the solution for both fluids simultaneously at each upcoming location (signified by the subindex $i$) since the heat transfer rate $q$ is a function of enthalpy, pressure and geometric parameters. Figure 3.2 summarizes the iteration sequence.

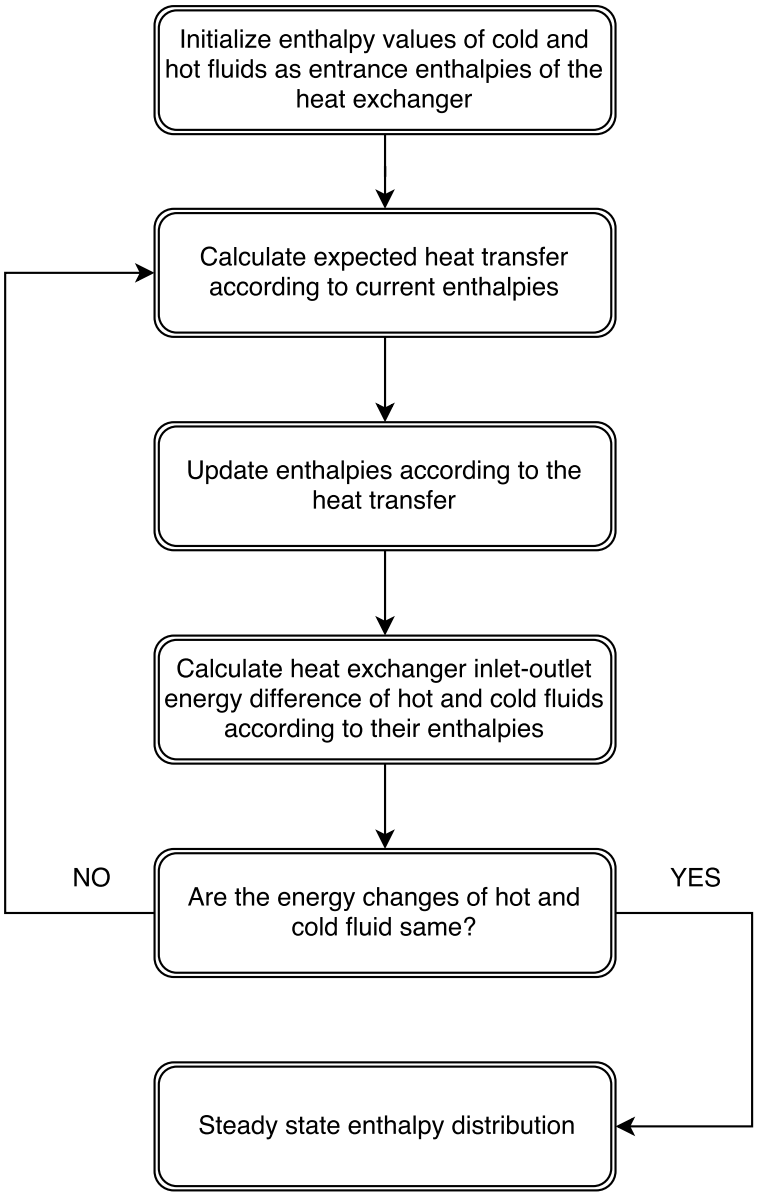


Figure 3.2. Steady state iteration flow chart

### 3.3. Discrete Dynamic Equations

The mass and energy conservation equations are solved via finite difference method using the formulation below:

- Mass conservation:

$$\frac{\rho_i^{t+1} - \rho_i^t}{\Delta t} = \frac{\rho_{i-1}^{t+1} v_{i-1}^t - \rho_i^{t+1} v_i^t}{\Delta x} \tag{3.2}$$

- Energy conservation:

$$\frac{\rho_i^{t+1} h_i^{t+1} - \rho_i^t h_i^t}{\Delta t} = \frac{\dot{m}_{i-1}^t h_{i-1}^{t+1} - \dot{m}_i^t h_i^{t+1} + q_i^t}{A \Delta x} \tag{3.3}$$

The general overview of the one dimensional central difference implicit scheme used is as follows:

$$(1 + \alpha_1)\sigma_i^{t+1} - \alpha_2 \sigma_{i-1}^{t+1} - \alpha_3 \sigma_{i+1}^{t+1} - \omega_i^t = \sigma_i^t \tag{3.4}$$

where $\sigma$ is the time dependent property , $\alpha_j$ are coefficients, $i$ is spatial indicator, $t$ is time step indicator, $\omega_i$ is the external action on $i^{th}$ cell. Then it can be expressed in matrix notation:

$$\Theta \Sigma^{t+1} - \Omega^t = \Sigma^t \tag{3.5}$$

$$\Sigma^{t+1} = \Theta^{-1}[\Sigma^t + \Omega^t] \tag{3.6}$$

Note that $\Sigma^0$ correspond to initial conditions. $\Theta$ is a square tridiagonal matrix (in 1-D flow) and it consists of $\alpha_j$.

For $N$ subcells, the corresponding matrices for mass conservation are given as:

$$\Theta = \begin{bmatrix} 1 & 0 & \dots & 0 & 0 \\ -\frac{\Delta t}{\Delta x} v_1^t & \frac{\Delta t}{\Delta x} v_2^t + 1 & \dots & 0 & 0 \\ \vdots & \vdots & \ddots & \vdots & \vdots \\ 0 & 0 & \dots & -\frac{\Delta t}{\Delta x} v_{N-1}^t & \frac{\Delta t}{\Delta x} v_N^t + 1 \end{bmatrix}_{N \times N} \tag{3.7}$$

The velocity at time t, $v^t$, is obtained by:

$$v^t = \dot{m}^t / \rho^t A \tag{3.8}$$

$$\Sigma = \begin{bmatrix} \rho_1 \\ \rho_2 \\ \vdots \\ \rho_N \end{bmatrix}_{N \times 1} \tag{3.9}$$

$$\Omega = \begin{bmatrix} 0 \\ 0 \\ \vdots \\ 0 \end{bmatrix}_{N \times 1} \tag{3.10}$$

And the matrices for the energy conservation are as follows:

$$\Theta = \begin{bmatrix} 1 & 0 & \dots & 0 & 0 \\ -\frac{\Delta t}{\Delta x} \frac{\dot{m}_1^t}{A \rho_2^t} & \frac{\Delta t}{\Delta x} \frac{\dot{m}_2^t}{A \rho_2^t} + \frac{\rho_2^{t+1}}{\rho_2^t} & \dots & 0 & 0 \\ \vdots & \vdots & \ddots & \vdots & \vdots \\ 0 & 0 & \dots & -\frac{\Delta t}{\Delta x} \frac{\dot{m}_{N-1}^t}{A \rho_N^t} & \frac{\Delta t}{\Delta x} \frac{\dot{m}_N^t}{A \rho_N^t} + \frac{\rho_N^{t+1}}{\rho_N^t} \end{bmatrix}_{N \times N} \tag{3.11}$$

$$\Sigma = \begin{bmatrix} h_1 \\ h_2 \\ \vdots \\ h_N \end{bmatrix}_{N\times 1} \tag{3.12}$$

$$\Omega = \begin{bmatrix} 0 \\ \frac{q_2^t \Delta t}{\Delta x A \rho_2^t} \\ \vdots \\ \frac{q_N^t \Delta t}{\Delta x A \rho_N^t} \end{bmatrix}_{N\times 1} \tag{3.13}$$

While the mass inside the heat exchanger changes, the mass flow rate distribution along the flow direction cannot be uniform. The mass flow rate value at the entrance to evaporator is defined as the boundary value $\dot{m}_1^t$, but subsequent mass flow rate values at the time t needs to be determined, $\dot{m}_i^t$, where $i = 2, 3.., N$. A flow chart of the time integration procedure is shown in Figure 3.3.

### 3.3.1. Iteration

For the $t^{th}$ time step, a mass flow rate vector, with length equal to the number of subcells, is created and its values are initialized with the entrance value:

$$\dot{m}_i^{t,1} = \dot{m}_0^t \qquad \text{for } i = 1, 2 \ldots, N \tag{3.14}$$

where the notation $\sigma_i^{t,j}$ is used to represent the $j$th iteration for the dynamic quantity at cell $i$ and time step $t$. For one step further in time, the density vector obtained from the mass flow rate dynamics and the thermodynamic state relations are compared, each one calculated respectively from the following equations:

$$\rho_i^{t+1,j} = \Delta t \left[ \frac{\dot{m}_{i-1}^{t,j} - \dot{m}_i^{t,j}}{A\Delta x} \right] + \rho_i^t \tag{3.15}$$

$$\rho_i^{t+1,j} = f(h^{t+1,j}, p^{t+1,j}) \tag{3.16}$$

If the density values obtained from Equations (3.15) and (3.16) differ by a significant amount, the mass flow rate values at time $t$ are updated using Equation (3.15) in order to satisfy density values given by Equation (3.16):

$$\dot{m}_i^{t,j+1} = -\frac{\rho_i^{t+1,j} - \rho_i^{t,j}}{\Delta t} A\Delta x + \dot{m}_{i-1}^{t,j} \tag{3.17}$$

A difference array $\delta^{t,j} = \{\delta_1^{t,j}\delta_2^{t,j} \ldots \delta_N^{t,j}\}'$ (where $Z'$ denotes the transpose of matrix $Z$) is constructed as

$$\delta_i^{t,j} = \dot{m}_i^{t,j+1} - \dot{m}_i^{t,j} \tag{3.18}$$

and the new iterative mass flow rate distribution array is constructed as:

$$\underset{\sim}{\dot{m}}^{t,j+1} = \underset{\sim}{\dot{m}}^{t,j} + \tau \underset{\sim}{\delta}^{t,j} \tag{3.19}$$

where $\tau$ is a small valued constant. The $\underset{\sim}{\dot{m}}$ denotes the array of the mass flow rate. The process continues until Equations (3.15) and (3.16) yield acceptably similar results for the vector. Then the final $\underset{\sim}{\dot{m}}^{t,j}$ becomes $\underset{\sim}{\dot{m}}^{t}$ and this is used in the time integration.

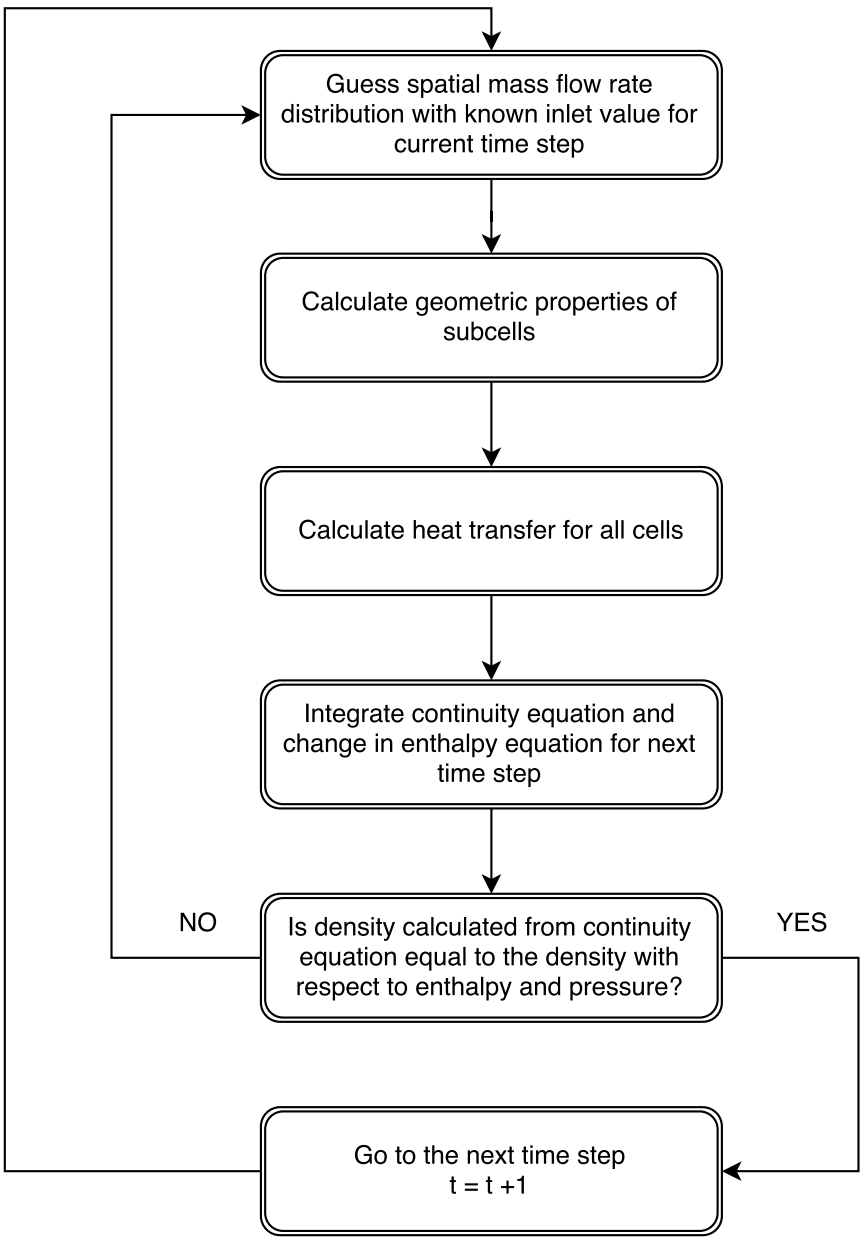


Figure 3.3. Time integration flowchart

# 4. SIMULATION AND EXPERIMENTAL VERIFICATION

## 4.1. Steady State Numerical Model

As a control step a steady state model of the heat exchanger is constructed to verify transient model's accuracy. The evaporator is selected as the test component. For the hot fluid (renolin) the enthalpy term in the governing equation is substituted with temperature term as $\Delta h = c\Delta T$. The geometry of the heat exchanger used in the experimental setup will be explained in detail in a later section.

### 4.1.1. Heat exchanger verification

Four steady state conditions are obtained by varying certain parameters. The dynamic model is set to an initial state and expected to visit all the four steady state consecutively. The Table 4.1 presents the inputs for the steady state conditions:

Table 4.1. Steady state inputs

| **Case** | **SS1** | **SS2** | **SS3** | **SS4** |
|---|---|---|---|---|
| **Ref. Pressure [bars]** | 15 | 19 | 19 | 19 |
| **Ref. Mass Flow Rate [kg/s]** | 0.15 | 0.15 | 0.10 | 0.18 |
| **Ref. Inlet Temperature [C]** | 12 | 12 | 12 | 12 |
| **Oil Inlet Temperature [C]** | 70 | 80 | 80 | 80 |
| **Oil Pressure [bars]** | 1 | 1 | 1 | 1 |
| **Oil Mass Flow Rate [kg/s]** | 2 | 2 | 2 | 2 |

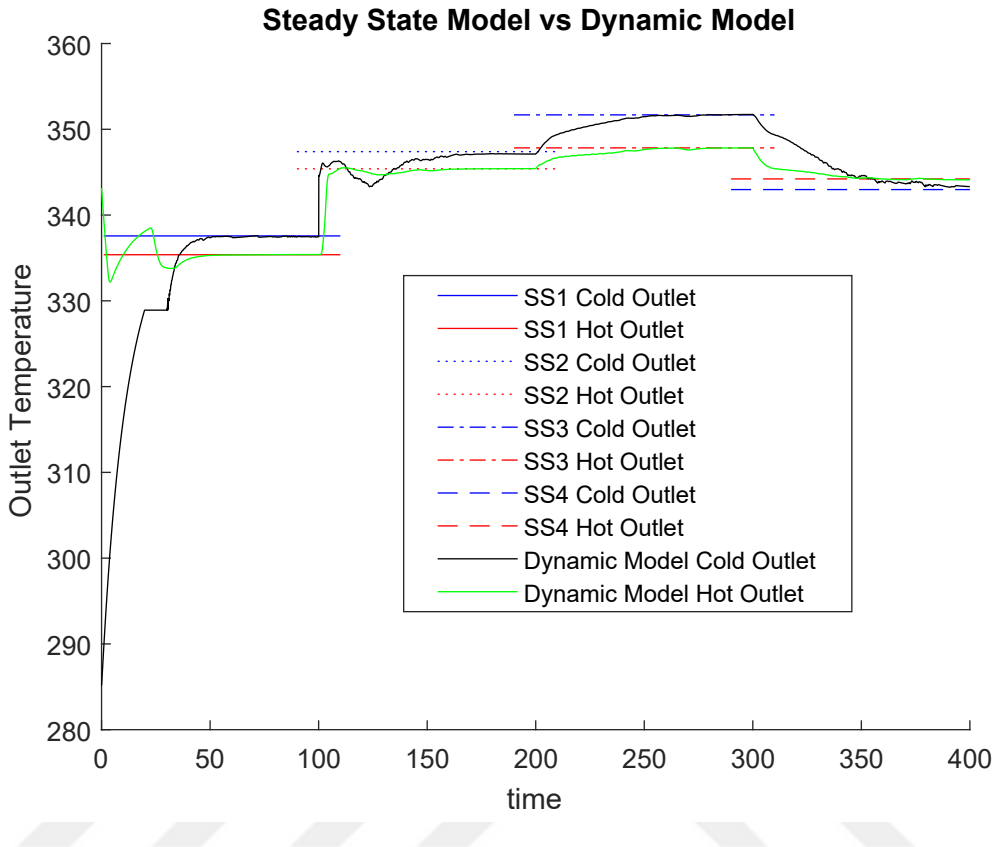


Figure 4.1. The comparison of the dynamic model result with the steady state results

The heat exchanger is divided into 100 subcells for the discrete model. The time step is chosen as 0.1 seconds. While the dynamic model is operating, the inputs are changed as previously explained every 100 seconds to give the dynamic model enough time to achieve the new steady state operating condition. The mass flow rate distribution is used as the indicator for having reached steady state: if outlet mass flow rate equals the inlet mass flow rate, than the mass inside the heat exchanger is constant.

The time variations of the outlet temperatures of r134a and renolin are presented in Figure 4.1. This figure clearly reveals that the dynamic model converges to the proper steady states.

## 4.2. The Influence of Mass Dynamics on the Numerical Model

The steady state solution is obtained when the time differential terms of the governing equation system equal to zero. In contrast, in a dynamic model, the transient behavior becomes as important as the steady state solution itself. The variation of the mass flow rate inside the heat exchanger along the flow direction has a strong influence on the model transients. To observe the effect of spatially variable mass flow rate, two simulations are conducted. First simulation is realized with the standart numerical models presented so far in the study, whereas the second simulation is realized with a so called quasi-dynamic model which simulates the system based solely on the energy balance equation. The purpose of the quasi-dynamic model is to estimate the major transient behavior more rapidly. If one aims to construct a controller algorithm, a quasi-dynamic model may be useful because of its speed. The dynamic model simulations are conducted with 60 and 100 subcells discretization. The conditions are preseted in the Table 4.2. The comparative results are illustrated as follows.

Table 4.2. Configuration properties

| Property | |
|---|---|
| **Ref. Pressure [bars]** | 15 |
| **Ref. Mass Flow Rate [kg/s]** | 0.15 |
| **Ref. Inlet Temperature [C]** | 12 |
| **Oil Inlet Temperature [C]** | 75 |
| **Oil Pressure [bars]** | 1 |
| **Oil Mass Flow Rate [kg/s]** | 2 |

Figure 4.2, which presents the results obtained for the 60 subcells system, shows that the response of the model with mass dynamics enabled is dramatically slower than the quasi-dynamic model. Figure 4.3 is the 100 subcells version of the figure 4.2. The important point is that both dynamic models converge nearly as expected. The quasi-dynamic model behaves like a upper bound for the dynamic model. Figure

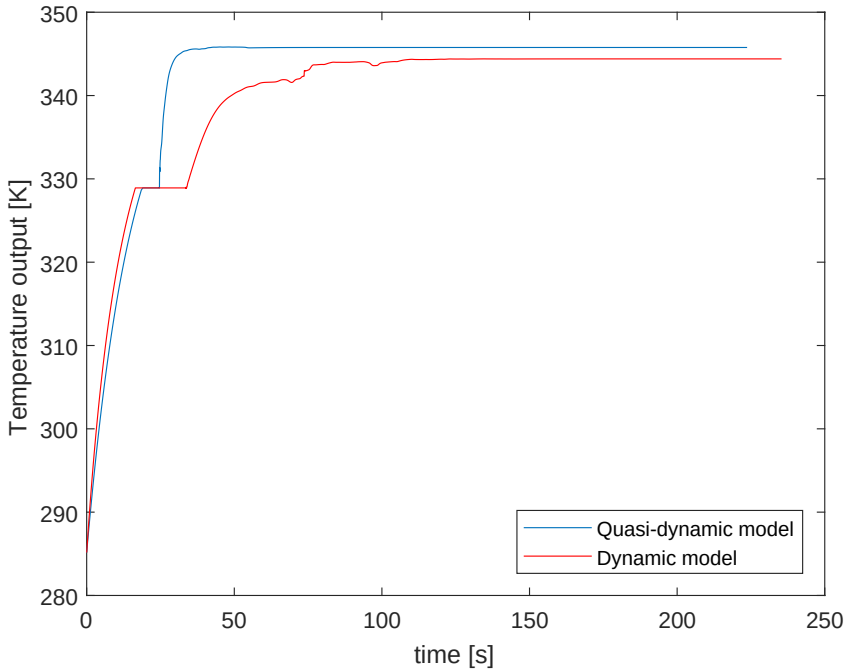


Figure 4.2. Comparison of the temperature outlets of dynamic model and quasi-dynamic model with 60 subcells.

4.4 represents the mass flow rate at the inlet and the outlet of the heat exchanger as obtained from the 60 subcells models while Figure 4.5 is that with the 100 subcells. When the simulation converges to a steady state, inlet and outlet mass flow rates are equal to each other since no variation in the enclosed mass inside the heat exchanger is expected. Figures 4.6 and 4.7 show the mass inside of the heat exchanger with 60 and 100 subcells, respectively, calculated both according to the mass flow rate difference and according to the density state of the working fluid.

### 4.2.1. The Momentum Balance Equation

It has been mentioned before that negligible pressure variation is expected along the flow direction. Therefore the momentum balance equation is neglected when constructing the dynamic model. On the other hand, it must be verified that the model does contradict the momentum equation so that the momentum balance check is required for the system. Recalling Equation (2.65) and setting the pressure variation in

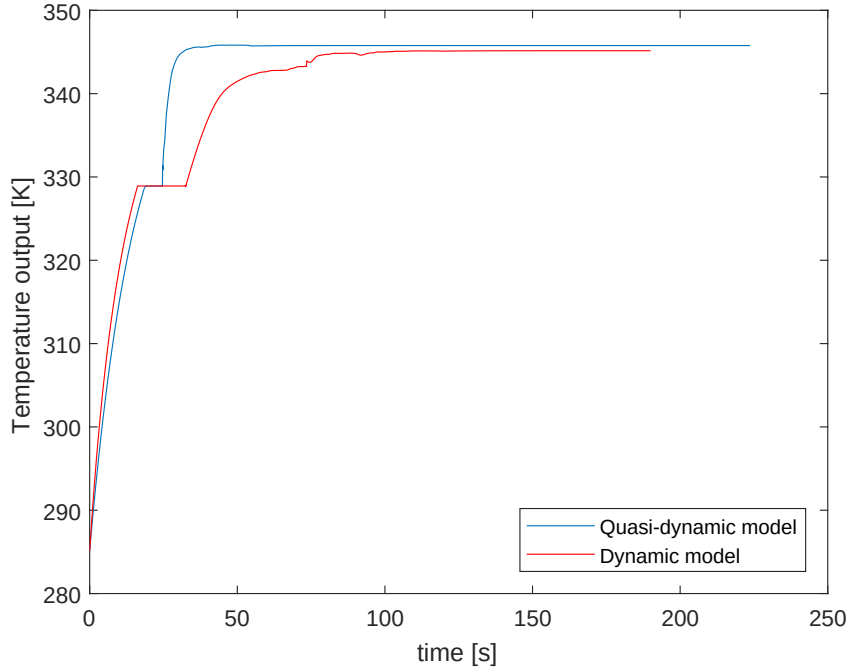


Figure 4.3. Comparison of the temperature outlets of dynamic model and quasi-dynamic model with 100 subcells.

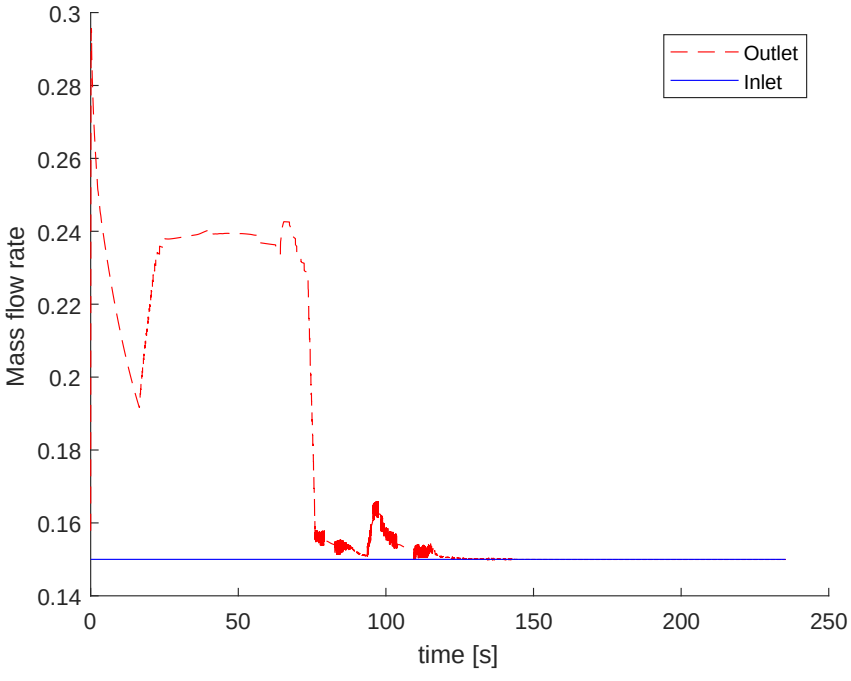


Figure 4.4. Inlet and outlet mass flow rate values versus time

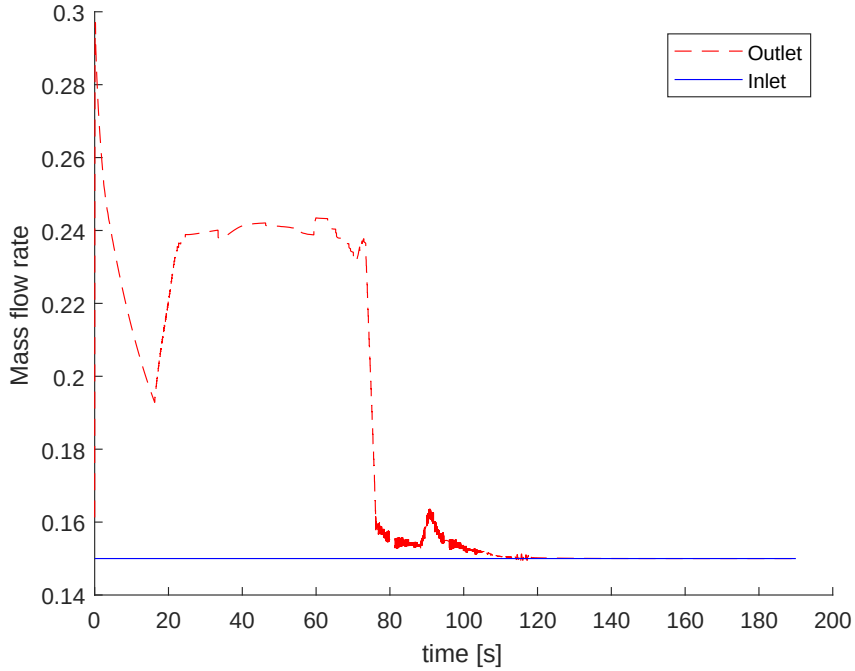


Figure 4.5. Inlet and outlet mass flow rate values versus time with 100 sub elements

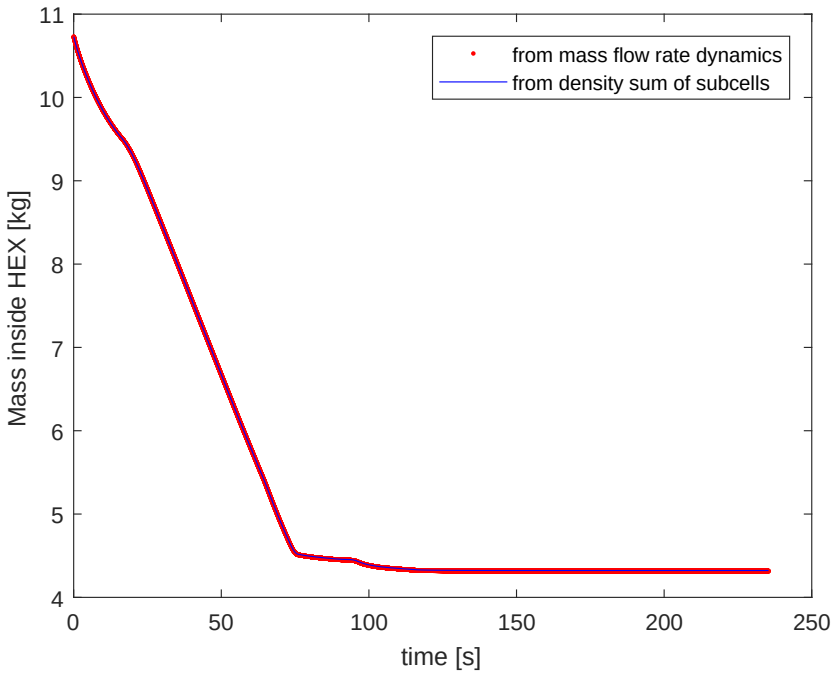


Figure 4.6. Change of the mass inside the heat exchanger versus time

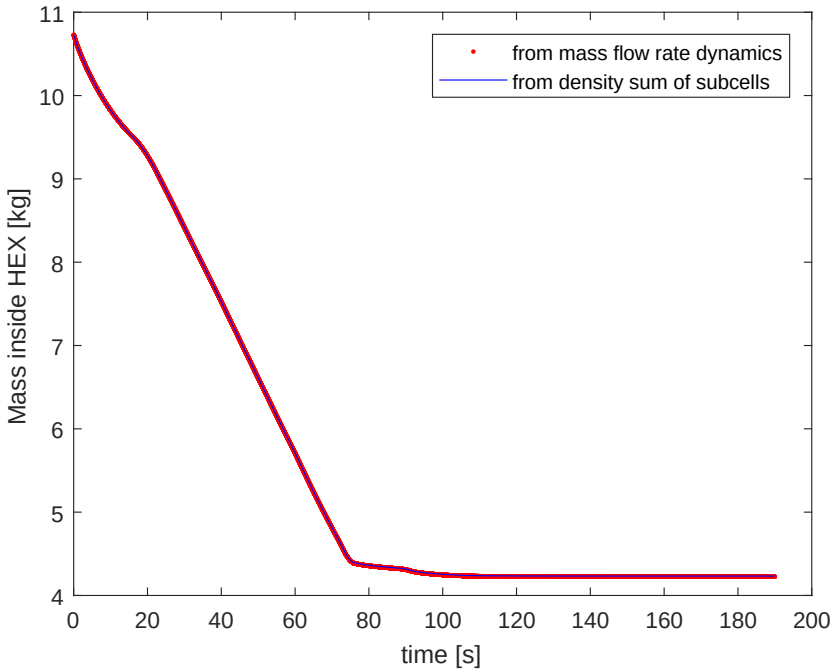


Figure 4.7. The time variation of the enclosed mass in the heat exchanger with 100 sub elements model

flow direction to zero, one gets the discretized equation:

$$0 = -\frac{\dot{m}_i^{t+1} - \dot{m}_i^t}{\Delta t} + \frac{(\dot{m}v)_{i-1}^t - (\dot{m}v)_i^t}{\Delta x} \tag{4.1}$$

The check is conducted using Equation (4.1) after the time histories are obtained with simulations. Figure 4.8 shows the momentum balance distribution along the flow direction and quality distribution along the flow direction at three instances during one simulation. First instant belongs to the beginning where the working fluid is in its single liquid phase at every cell, second instant belongs to the evaporation stage when liquid has liquid and gas-liquid phases, third instant is when system is close to the steady state, when liquid, gas-liquid, and gas phases are all present. It is observed that the calculated flow satisfies momentum balance when it is in single phase (liquid or gas); however, slight deviations exist in the two-phase zone, most likely as a result of the strong variation in the density. Another simulation is conducted where heat exchanger discretized into 100 sub cells. According to the results,less deviation from the momemtum balance is observed. The figure 4.9 shows the spatial momentum

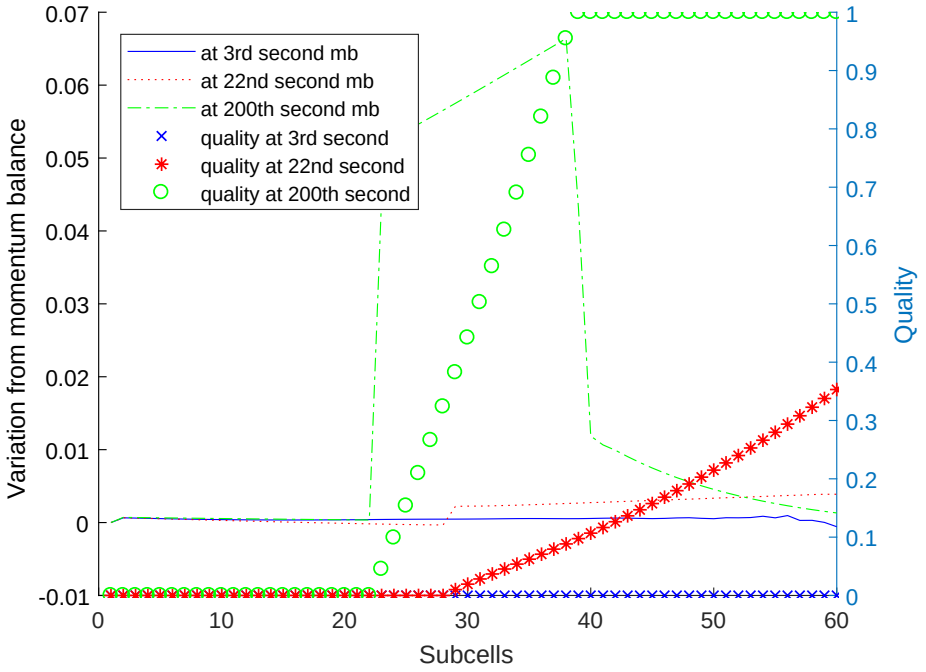


Figure 4.8. Spatial distributions of momentum balance and quality at three instants with 60 sub elements

balance at three instances during the simulation.

### 4.3. Utilization of an Low Pass Filter in the Dynamic Model

A low pass filter for the heat transfer rate is implemented in the model to filter the high frequency oscillations observed in the heat transfer rate and to increase the stability of the model. The transfer function of the filter in laplace domain is shown below:

$$H(s) = \frac{y(s)}{u(s)} = \frac{1}{as+1} \tag{4.2}$$

where, $y$ is signal output, $u$ is signal input and $a$ is a filter parameter, that needs to be optimized according to the signal values and the time step, $\Delta t$. The inverse Laplace transformation of the equality yields into:

$$a\dot{y}(t) + y(t) = u(t) \tag{4.3}$$

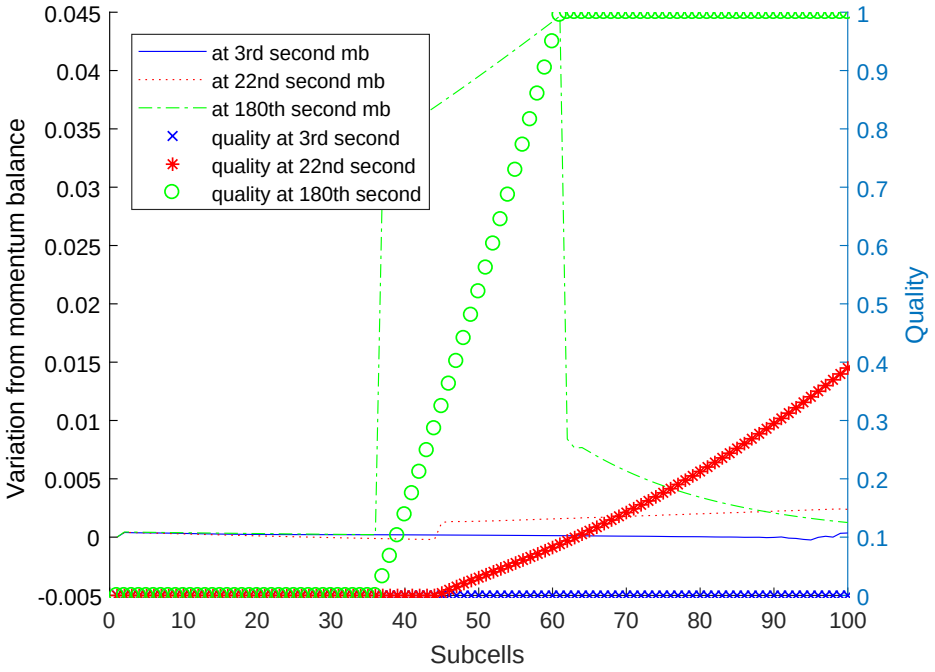


Figure 4.9. Spatial distributions of momentum balance and quality at three instants with 100 sub elements

$\dot{y}(t)$ is calculated by:

$$\dot{y}(t) = \frac{y(t) - y(t - \Delta t)}{\Delta t} \tag{4.4}$$

finally, the signal output $y(t)$ equals:

$$y(t) = \frac{a}{a + \Delta t} y(t - \Delta t) + \frac{\Delta t}{a + \Delta t} u(t) \tag{4.5}$$

$u(t)$ is selected as $q_i(t)$, and, $y(t_0) = u(t_0)$ for the first time step. Such a filter, however, causes a time lag in the system and therefore may not useful under all circumstances. This filter is only used in this section of the study for the purpose of showing its effects on transient outcomes and the convergence of the system.

The heat transfer rate distribution over the heat exchanger, when the liquid phase, the two-phase and the gas phase are all present, is illustrated in Figure 4.10.

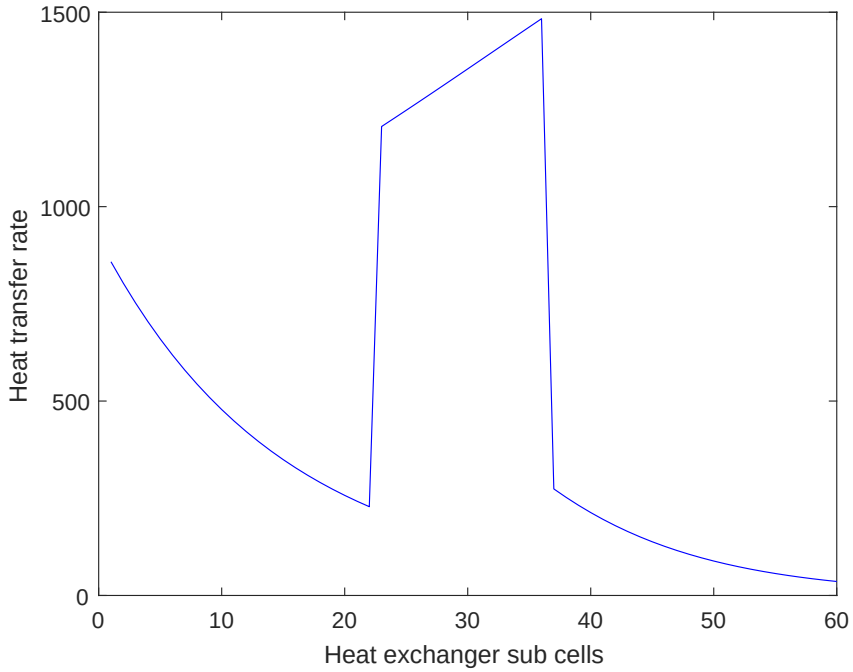


Figure 4.10. Spatial heat transfer rate distribution in the steady state condition.

The heat transfer time history of one subcell, which is at gas phase in the steady state condition, is given in Figure 4.11.

The results reveal a great difference in the heat transfer rate between single phase and two phase conditions. This difference causes high frequency oscillations in the transients. Simulating the same system with the quasi-dynamic model introduced previously, with an exaggerated time step ($dt = 3$ seconds) to see the effect clearly and using 60 subcell discretization, it is seen in Figure 4.12 that the system does not converge initially; when the filter is activated after 100 seconds, convergence is obtained.

Moreover, when the dynamic simulation is run with a time step of $dt = 0.5$ seconds, the outlet temperature time histories obtained with and without the filter are presented in the Figure 4.13.

The filtered and unfiltered heat transfer coefficient of the same subcell is presented in Figure 4.14. The simulation is expected to be unstable with the given time step,

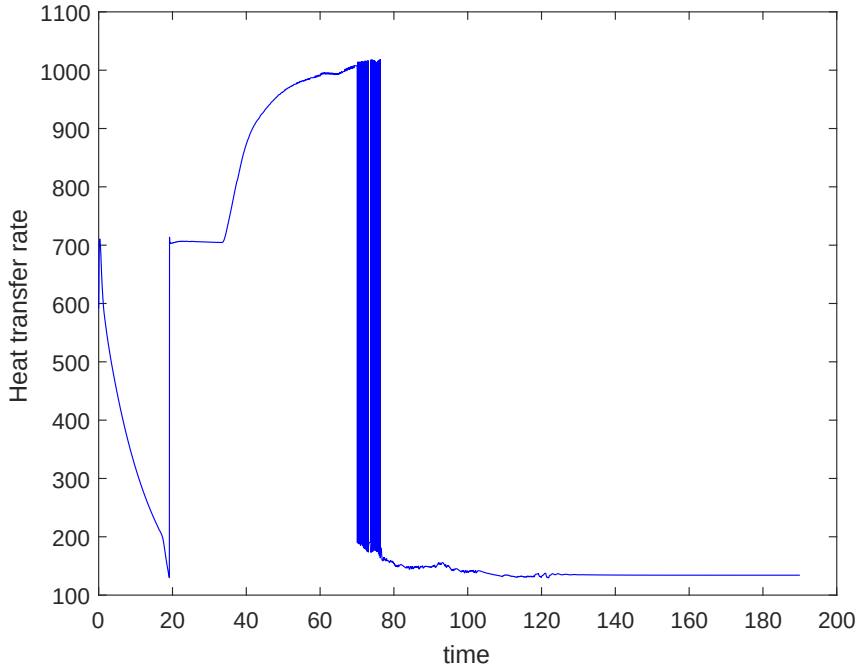


Figure 4.11. Heat transfer rate time history of a subcell, including phase change.

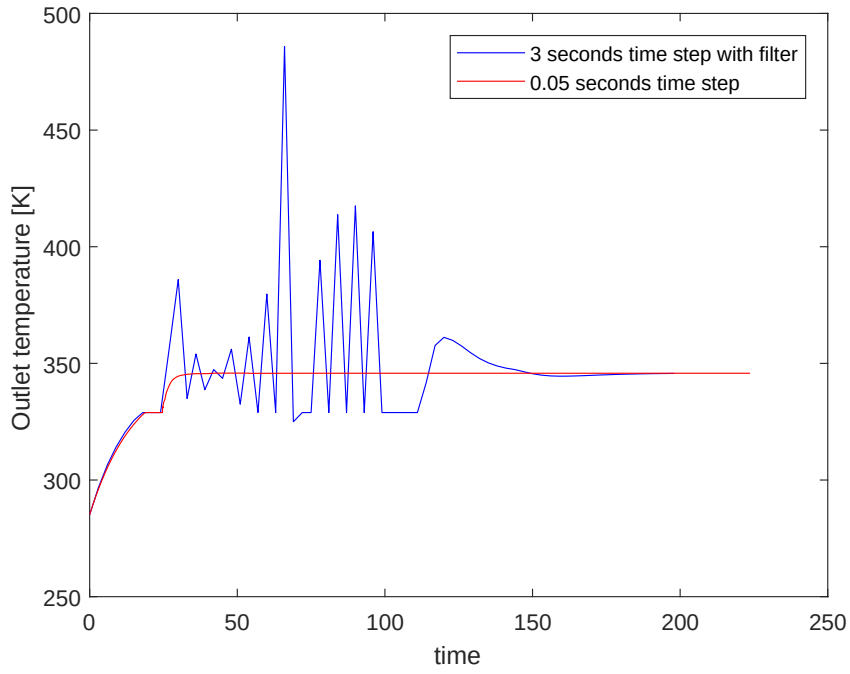


Figure 4.12. The stabilizer effect of low pass filter on an unstable quasi-dynamic simulation.

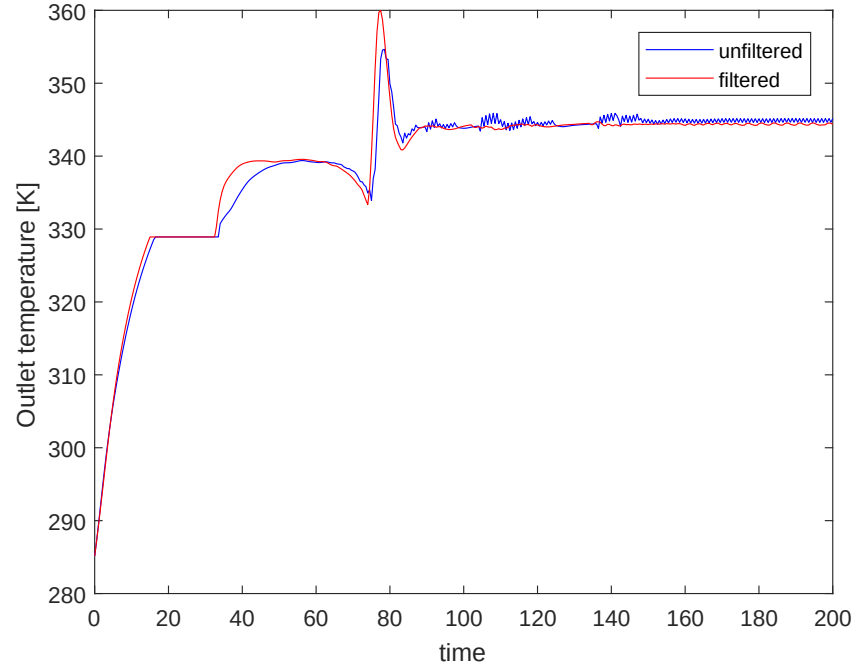


Figure 4.13. Comparative results of an unstable dynamic simulation.

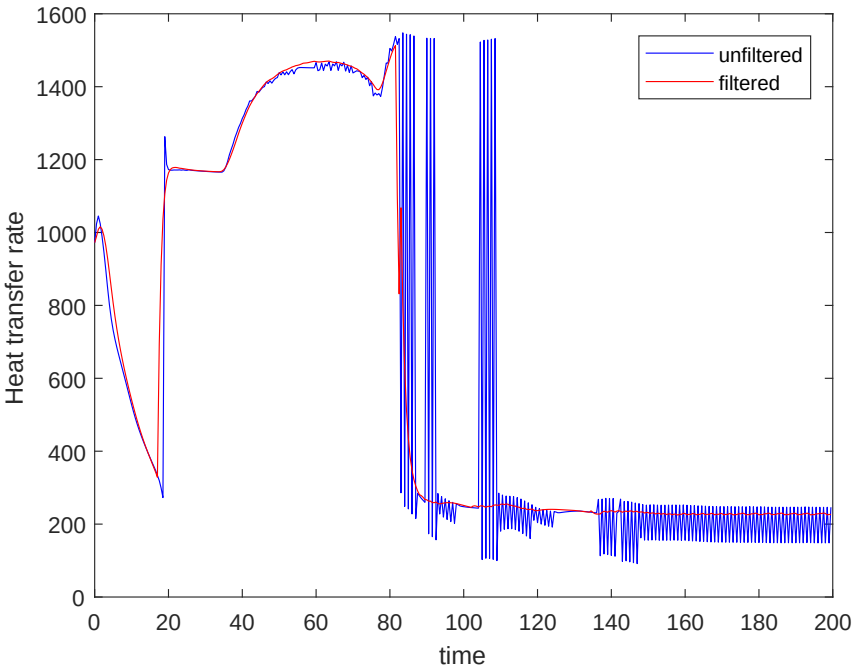


Figure 4.14. The comperative heat transfer rate time history of same sub cell, which encounters phase change

however, employing a low pass filter increases the model's stability. With a careful investigation before implementation, heat transfer rate time history is obtained smoothly leading to more realistic results. The filter also introduces a lag for the transients, and, causes unrealistic peaks since its algorithm carries information from previous time step. Therefore, it would be more useful when computational time needs to be short, and, when the transients are less important than the steady state results. Hence, the filter will not be used further in this study since stability is achieved with small time steps and a short computational time is not vital for the current purposes.

## 4.4. Bogazici University BURET Laboratory

The Renewable Energy Technologies Laboratory (BURET) located at the Kilyos Campus of Boğaziçi University offers a great opportunity to verify the applicability of the developed model. Experiments were conducted at BURET with two main goals: the first goal was to reach a steady state operating condition and maintaining that condition, and the second goal was to change the ORC system variables and observe their influence on the operating system as the system reached another steady state operating condition.

### 4.4.1. Experimental setup

The ORC construction at BURET contains the following components: three heat exchangers (evaporator/condenser/chiller), one centrifugal pump, hot oil supply, and cold water supply. A schematic presentation of the system is presented in Figure 4.15. For monitoring of the working fluid (r134a), there are pressure and temperature sensors located at inlets and outlets of the heat exchangers and the pump, and there is a mass flow rate sensor between the pump and the evaporator. Hot oil temperatures at the inlet and outlet of the evaporator are measured. Hot oil (renolin) flows at a constant mass flow rate. There are also temperature sensors located at the inlets and outlets of the condenser and the chiller to monitor the cold water flow. The mass flow rate of the cold water is controlled manually by valves. The mass flow rate of the working fluid is also controllable via a by-pass valve located after the pump, which enables adjustments

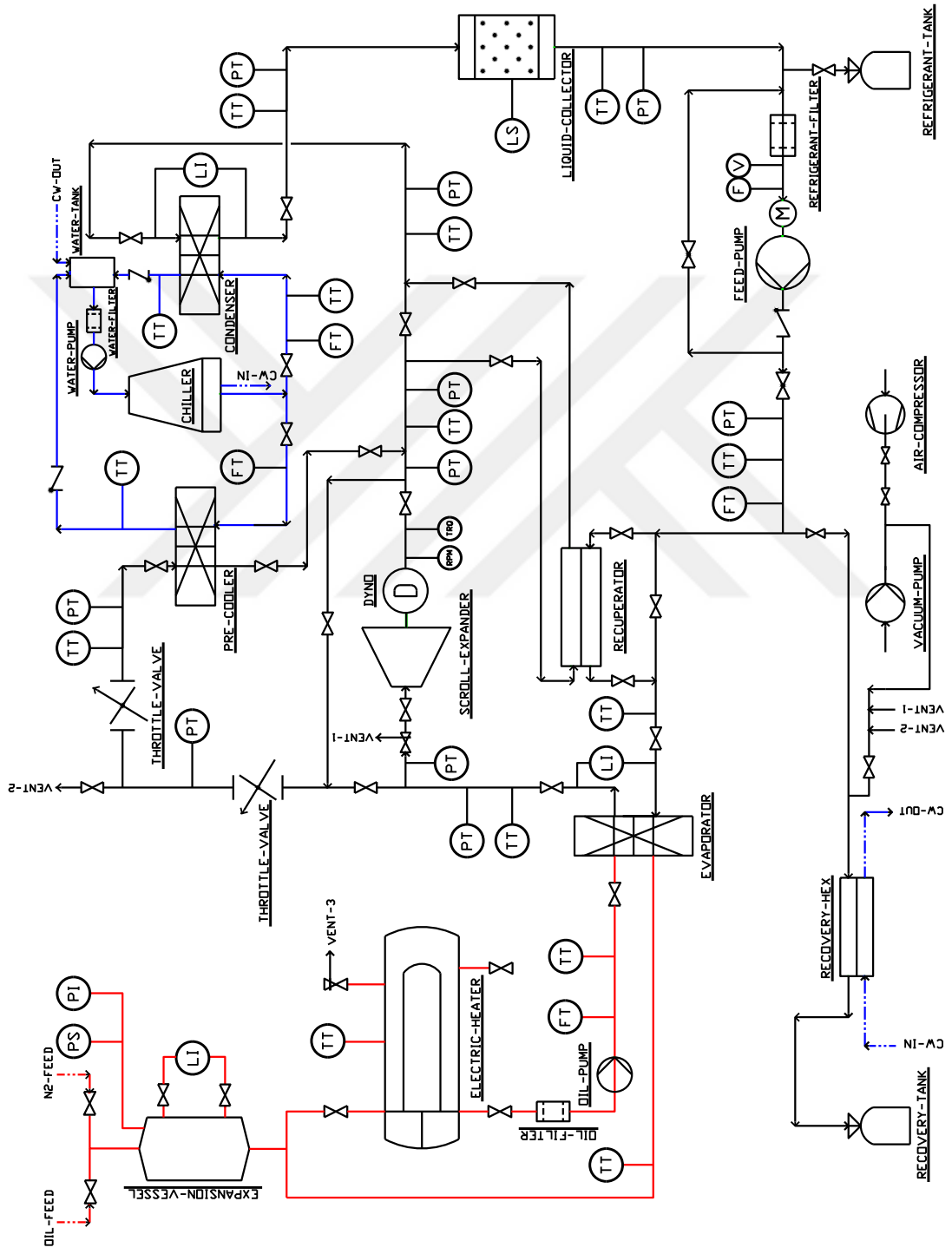


Figure 4.15. PID of the experiment setup

for achieving the desired mass flow rate independent from performance curve of the pump.

### 4.4.2. Heat exchanger verification

Figure 4.16. Heat Exchanger

The heat exchangers of the ORC are manufactured by Ekin Endustriyel with product code MB09. The picture of the heat exchanger in use is given in Figure 4.16. According to the information provided by the manufacturer, geometric properties of the evaporator and condenser are as follows:

- $A_{tr} = 0.095m^2$
- $L_h = 615mm$
- $L_w = 188mm$
- $L_p = 2.4mm$
- $t_p = 0.2mm$
- $l_v = 515mm$
- $l_h = 95mm$
- $D_p = 40mm$

For the evaporator:

- $N_H = 39$
- $N_C = 40$

For the condenser and chiller:

- $N_H = 34$
- $N_C = 33$

where, as before, $N_H$ and $N_C$ indicate the number of channels for the hot and the cold fluids, respectively. According to Equation (2.61) ( [37]),

- $D_{hyd} = 3mm$

The numerical dynamic ORC model is constructed using numerical models of the heat exchangers. The analysis in the previous section indicates that the dynamic methodology and numerical integration are consistent and the dynamics may be reliably simulated. The verification with experimental data would help to further increase the confidence in the model as well as providing an objective basis to discuss the effectiveness of the heat transfer correlations in representing the physical system well and to discuss whether the fluid properties are calculated properly according to the thermodynamic state. In the numerical simulations, the Martin correlation [44] is used for the single phase and the Gungor and Winterton correlation [37] is used for the two phase zones. The verification is conducted via the following procedure:

- The inlet temperatures of hot and cold fluids are inputs,
- The mass flow rate and the system pressure are provided by the pump and they are also inputs,
- Outlet temperatures of hot and cold fluids are calculated by numerical model and compared by the experimental results.

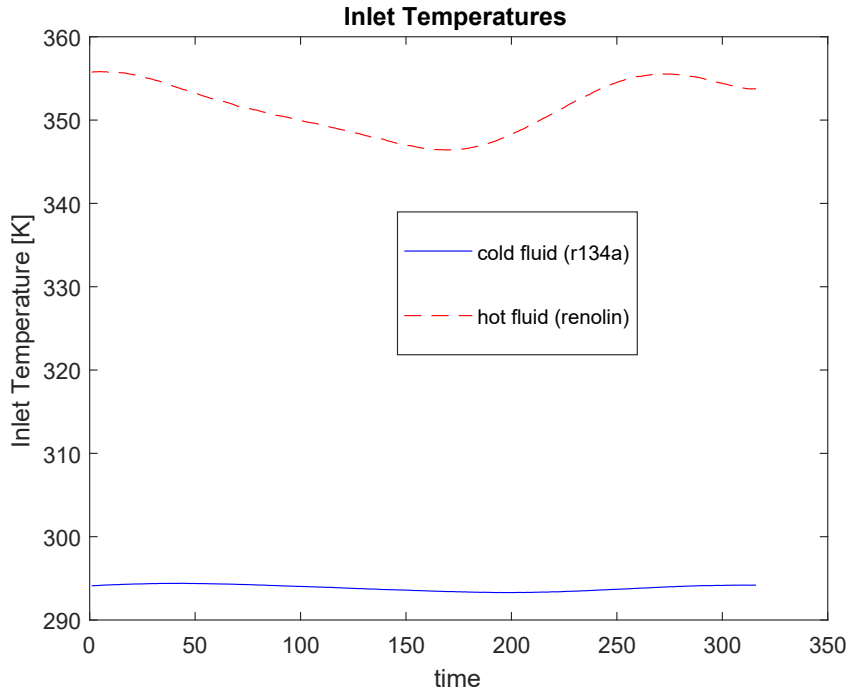


Figure 4.17. Inlet temperatures of fluids versus time.

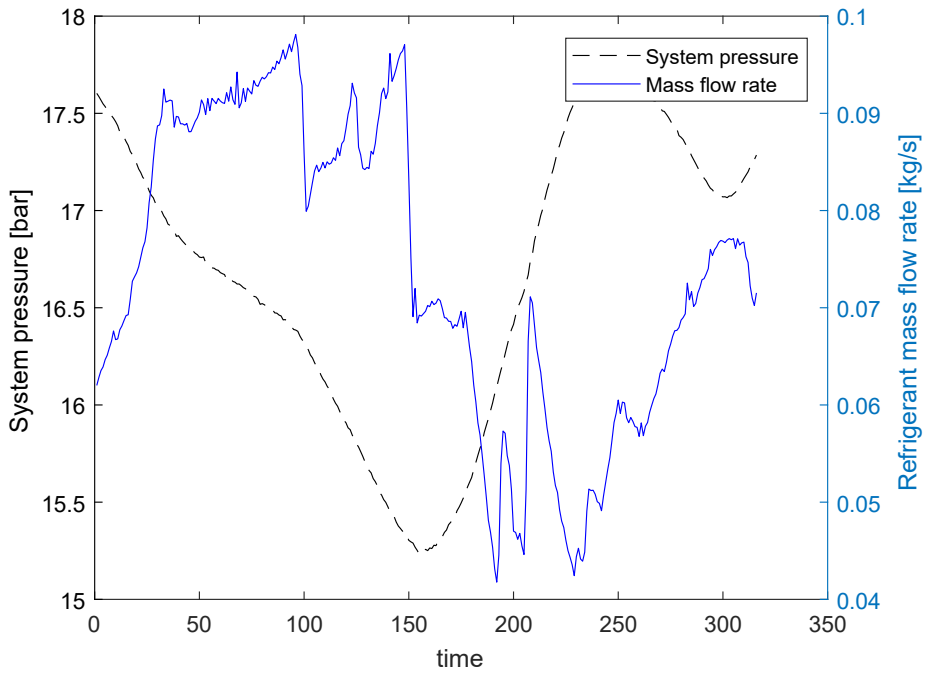


Figure 4.18. The mass flow rate and system pressure versus time.

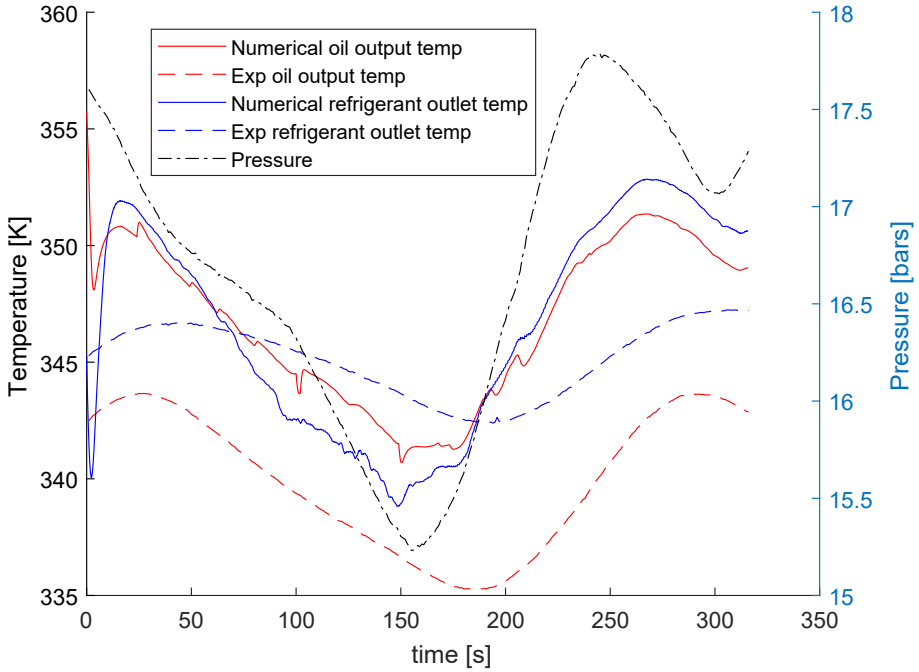


Figure 4.19. Outlet temperatures vs time.

In the experiment, data is sampled at a rate of 1 Hz so that the inputs change once in every second. On the other hand the time step is chosen as $dt = 0.1$ seconds for the numerical model such that the inputs are kept constant for 10 consecutive time steps. The inlet temperatures are plotted in Figure 4.17, the mass flow rate of r134a and the system pressure are plotted in Figure 4.18. The outlet temperature time histories of the fluids are shown in Figure 4.19.

Results of an energy balance analysis combined with heat transfer rate are plotted in Figure 4.20. The energy change rate is calculated for each time step based on the difference of the inlet and outlet fluid temperatures. Since heat loss to the surroundings is neglected, the energy change rate of both fluids are expected to be same with the heat transfer rate in the steady state condition; on the other hand, since the inputs are changing only once in every second, a converging behavior is to be expected rather than an exact equality. The refrigerant mass inside the heat exchanger and fluid level of the evaporator on a scale between 0 and 1 is shown in Figure 4.21, which is expected to match with the real experiment's level gauge if it were recorded.

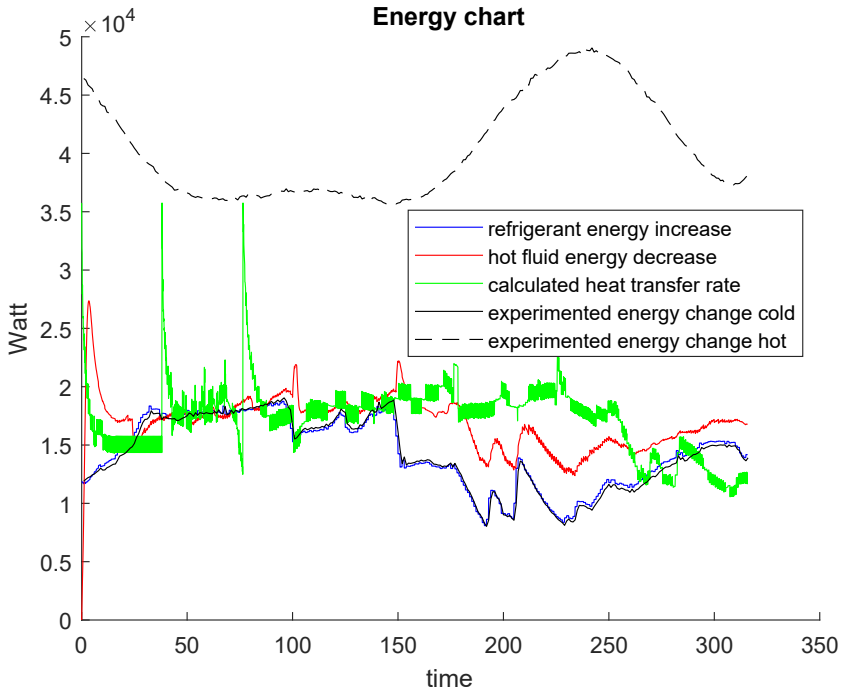


Figure 4.20. Energy balance analysis

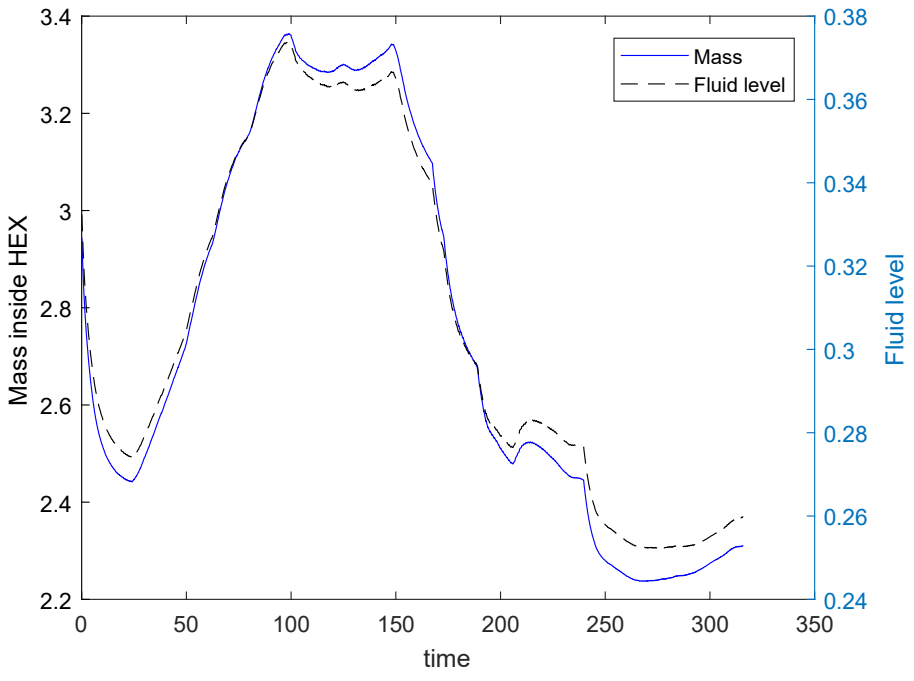


Figure 4.21. Refrigerant mass and fluid level

According to the results, the energy change rates of fluids in the numerical constructed model are consistent with each other and with the estimated heat transfer rate. There is, however, an inconsistency in the experimental results, since the heat loss of the hot fluid is greater than the energy gained by cold fluid. It may poin out a leakage in the experimental setup.

Since the refrigerant outlet temperature of the numerical model and the experimentally observed temperature differ in the acceptable range and the general dynamic behavior is replicated successfully, we conclude that the numerical model of the heat exchanger is acceptable and can be used in the numerical model of the entire ORC system.

### 4.4.3. Combined System verification

The solution of the governing dynamic equations and the accuracy of heat transfer correlations for heat transfer rate calculations are studied in the previous sections. A complete system investigation is also needed to show if the numerical model's reaction to the changing inputs represent real case. In this section a different experimental data will be used for the numerical simulation of the combined pump-evaporator-condenser system. The time dependent inputs of such the system are the evaporator side inlet temperatures of the cold (r134a) and the hot (renolin) fluids, the condenser side inlet temperature of the cold fluid (water) and its mass flow rate, the system pressure, and the mass flow rate of the working fluid (r134a). The mass flow rate of renolin is constant at 1.6 kg/s. The condenser side inlet temperature of the hot fluid (r134a) is taken as the outlet temperature of the evaporator. Moreover, the system pressure is reduced to around 7 bars after the evaporator by a pressure reducing valve present in the experimental setup. During the experiment, two segments are observed in which the system operates stable. The data gathered from those two segments will be presented below. The sampling rate of the experiment is 1 Hz and time step for numerical simulations is 0.5 seconds.

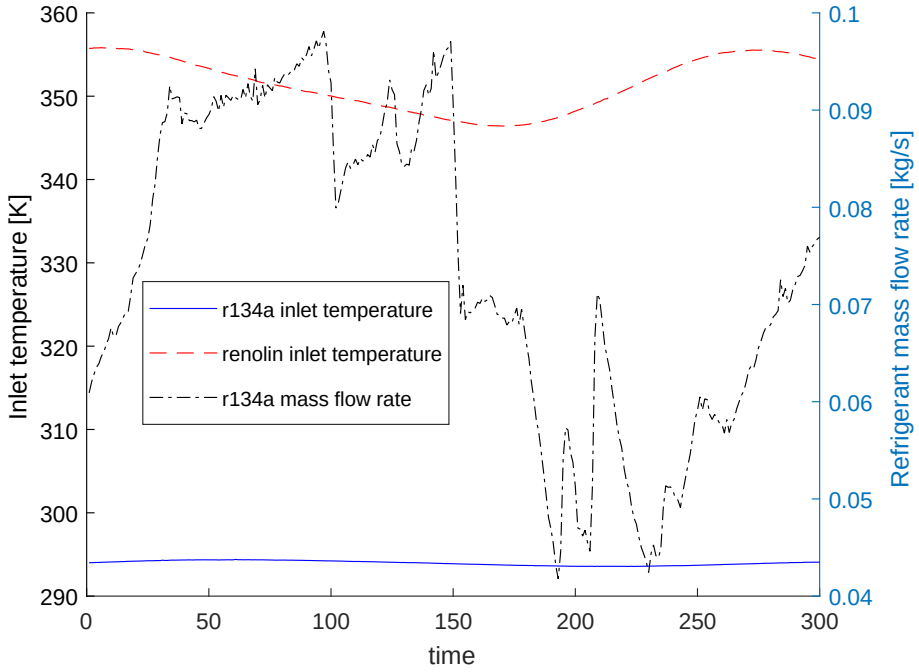


Figure 4.22. Evaporator inputs (first segment).

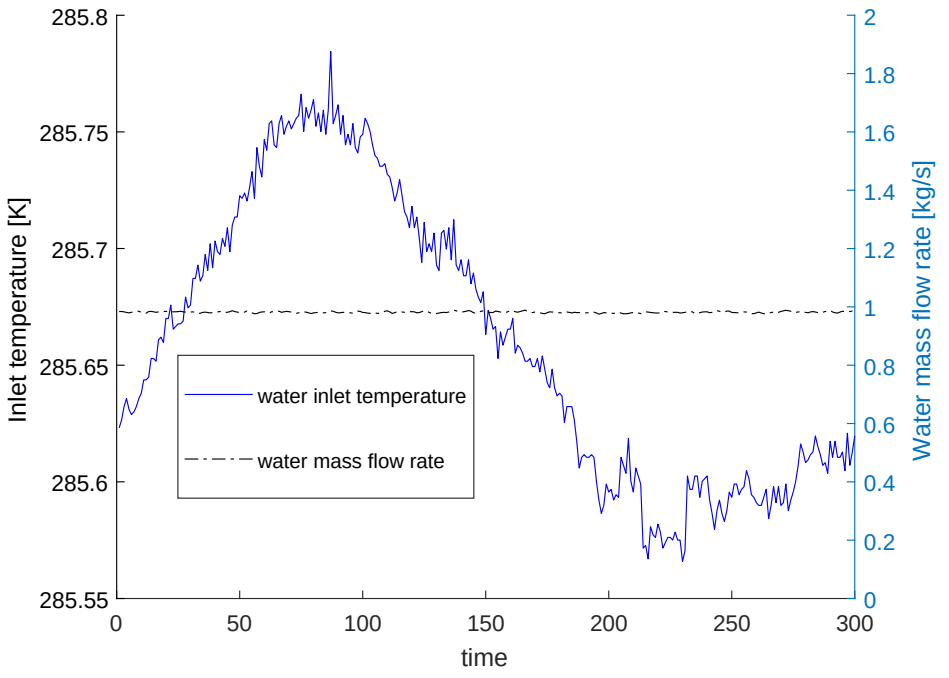


Figure 4.23. Condenser inputs (first segment).

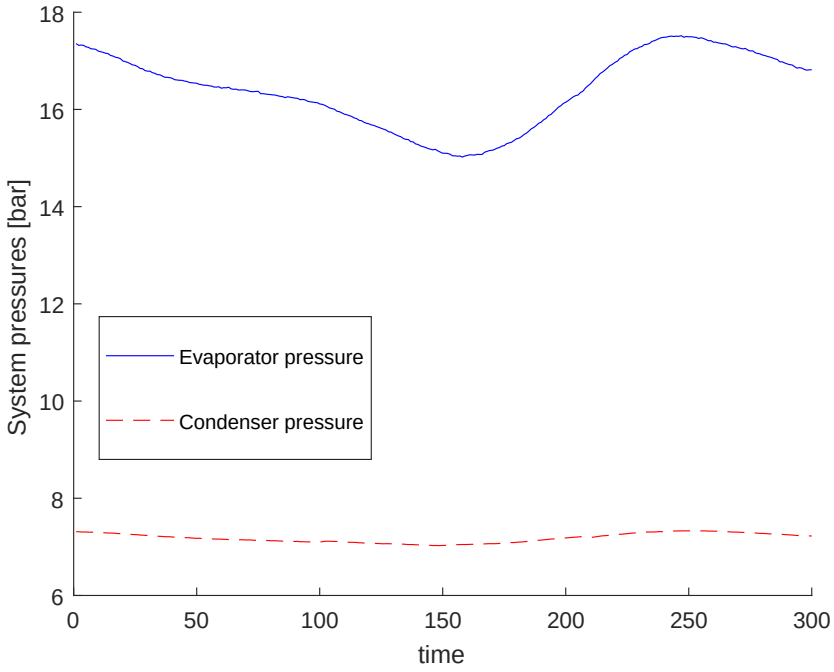


Figure 4.24. System pressures (first segment).

4.4.3.1. First segment. The inlet temperature of the evaporator side and the inlet mass flow rate of r134a are presented in Figure 4.22; the inlet temperature and the mass flow rate of water in the condenser side are presented in Figure 4.23. Time variation of the evaporator and condenser pressures are shown in Figure 4.24.

The evaporator side outlet temperatures obtained in the simulations are presented in Figure 4.25, and the evaporator energy balance combined with the estimated heat transfer rate is presented in Figure 4.26. The condenser side outlet temperatures and the condenser energy balance are shown respectively in Figure 4.27 and Figure 4.28.

4.4.3.2. Second segment. The inlet temperatures of the evaporator side and the inlet mass flow rate of r134a are presented in Figure 4.29; the inlet temperature and the mass flow rate of water in condenser side are presented in Figure 4.30. Time variation of the evaporator and condenser pressures are given in Figure 4.31.

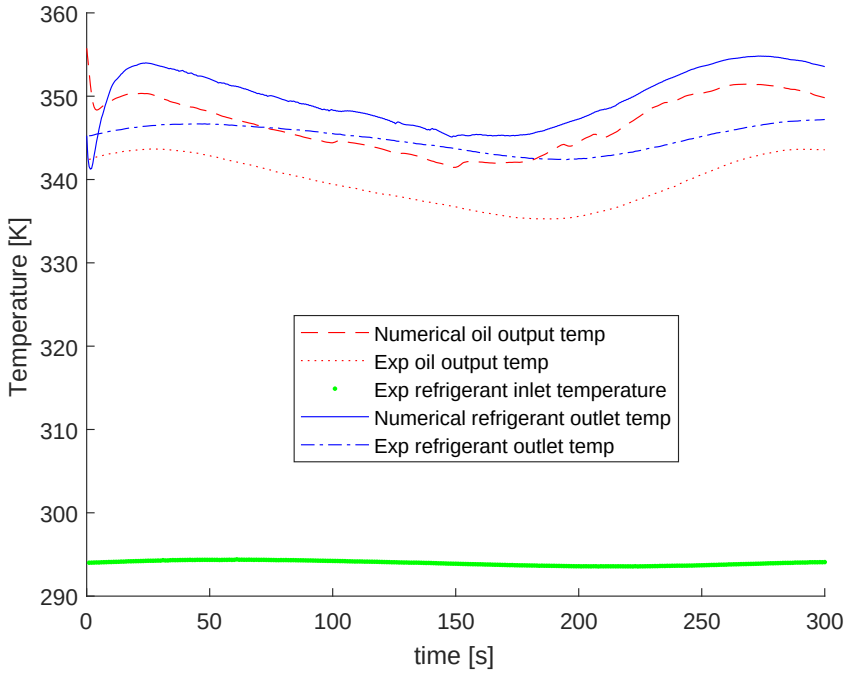


Figure 4.25. Evaporator outputs (first segment).

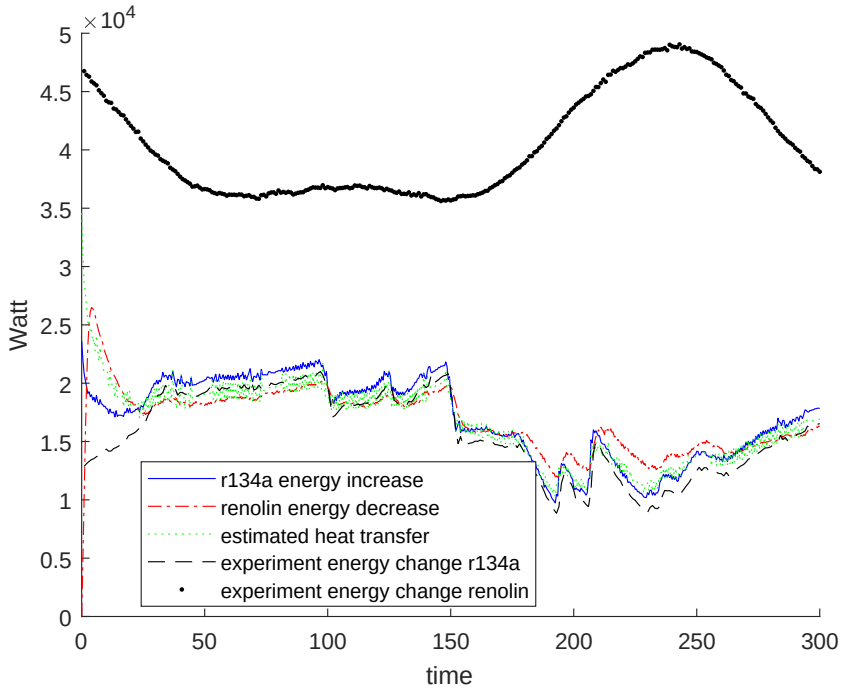


Figure 4.26. Evaporator energy balance (first segment).

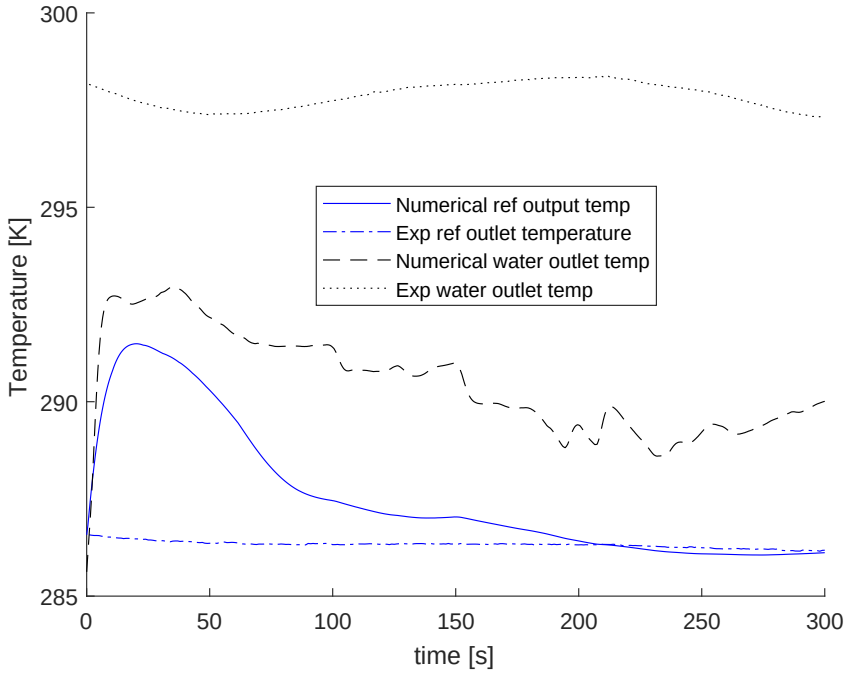


Figure 4.27. Condenser outputs (first segment).

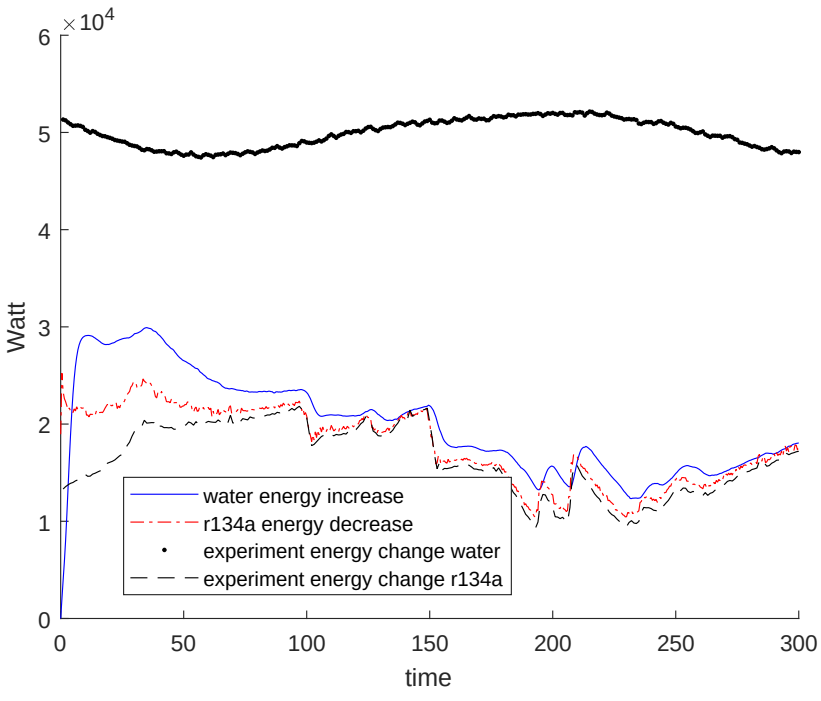


Figure 4.28. Condenser energy balance (first segment).

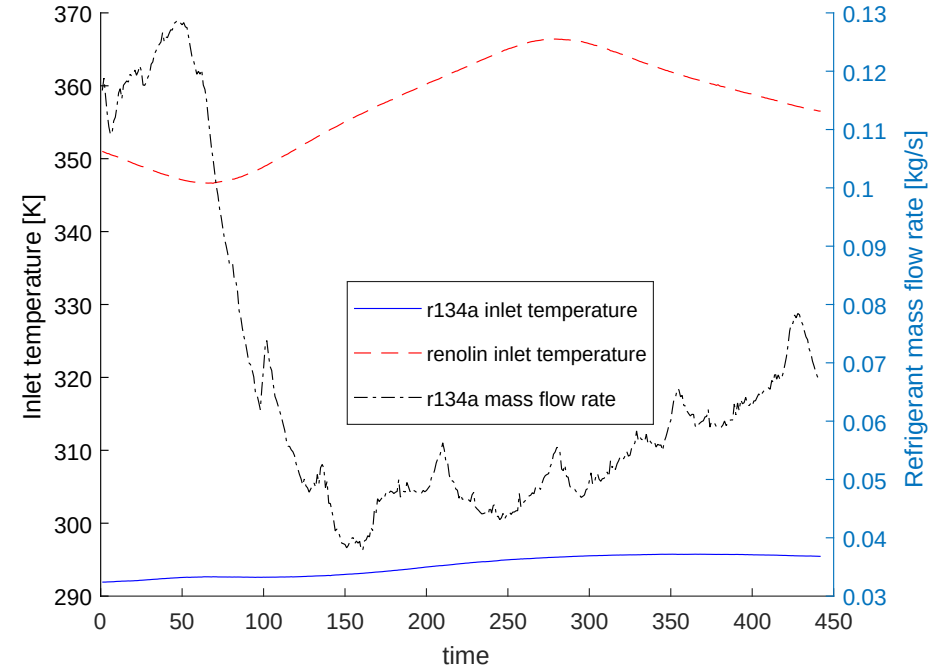


Figure 4.29. Evaporator inputs (second segment).

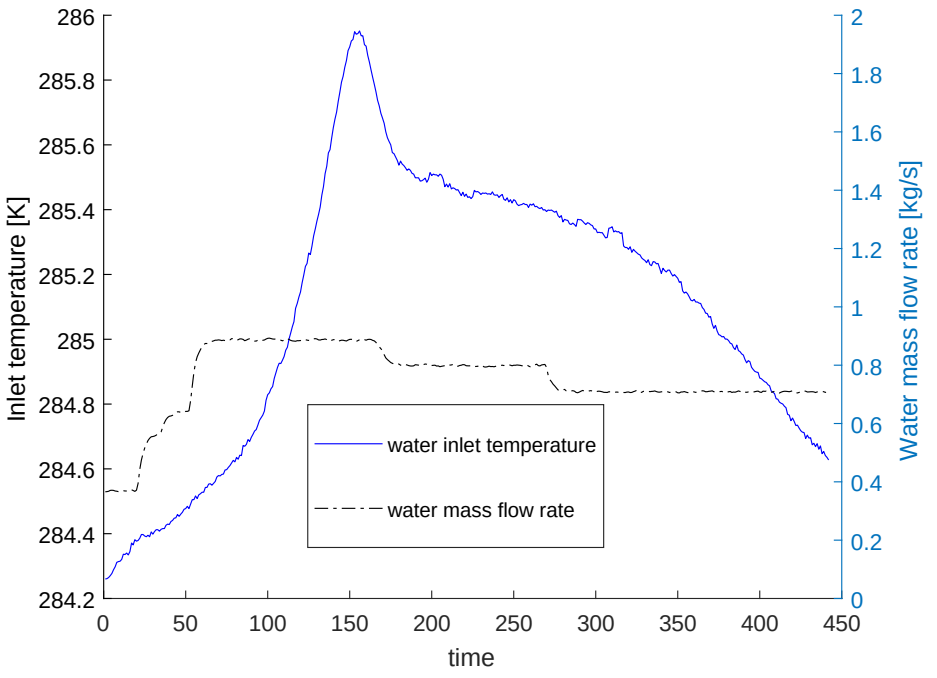


Figure 4.30. Condenser inputs (second segment).

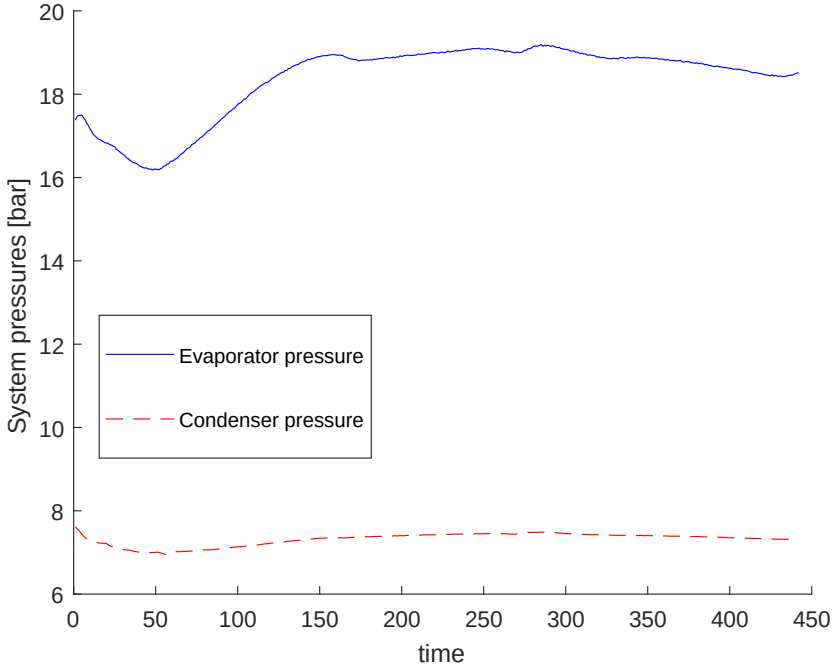


Figure 4.31. System pressures (second segment).

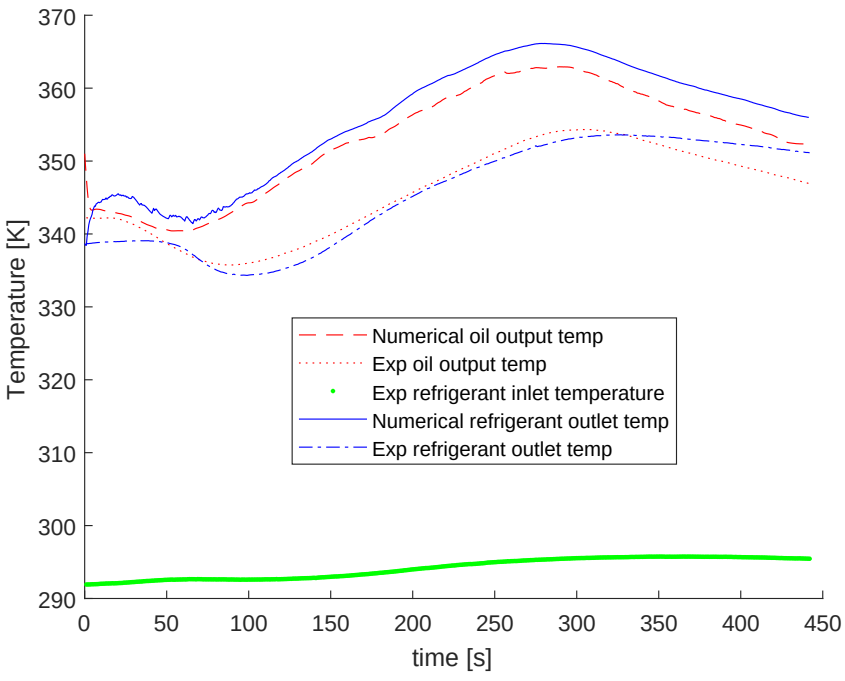


Figure 4.32. Evaporator outputs (second case)

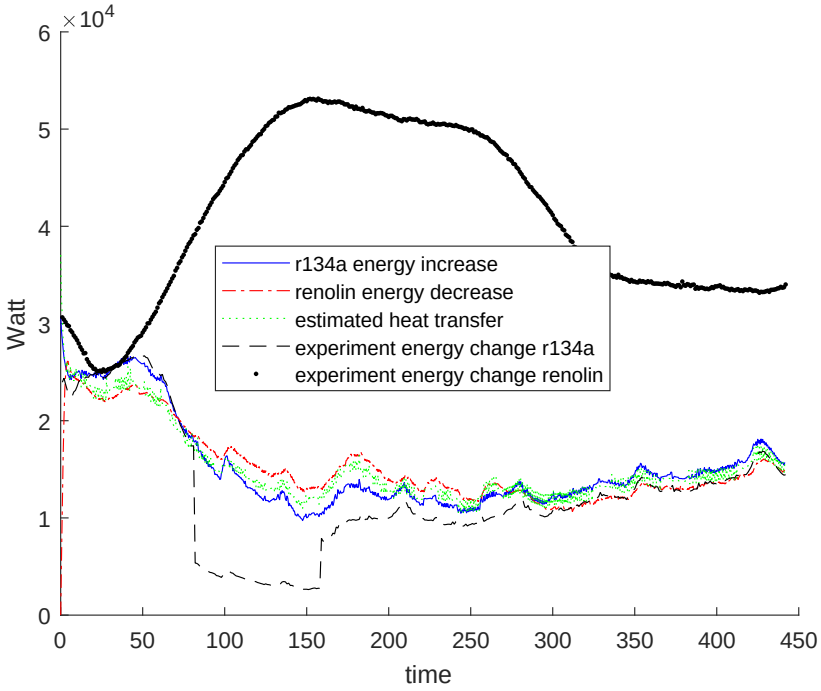


Figure 4.33. Evaporator energy balance (second case)

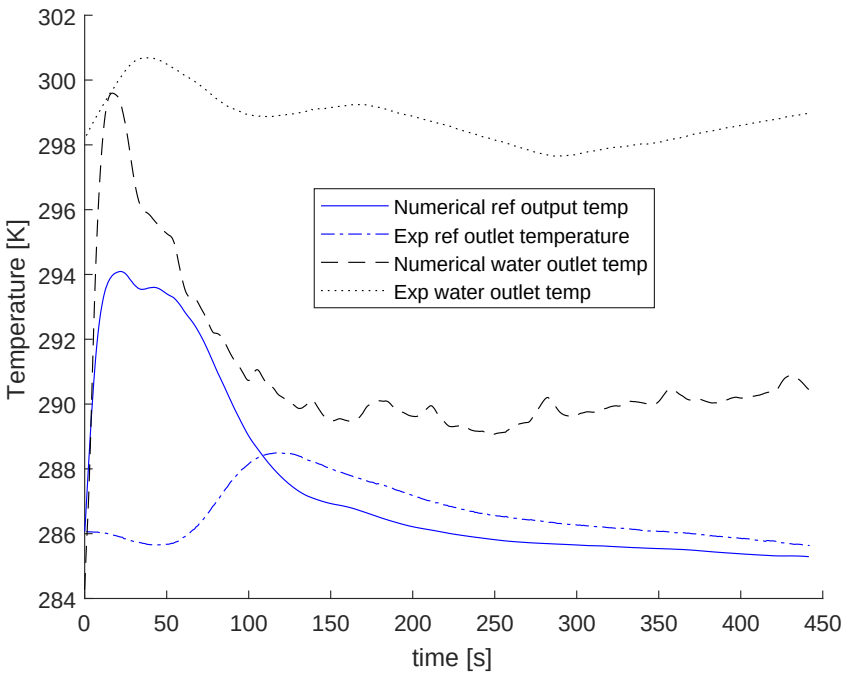


Figure 4.34. Condenser outputs (second case)

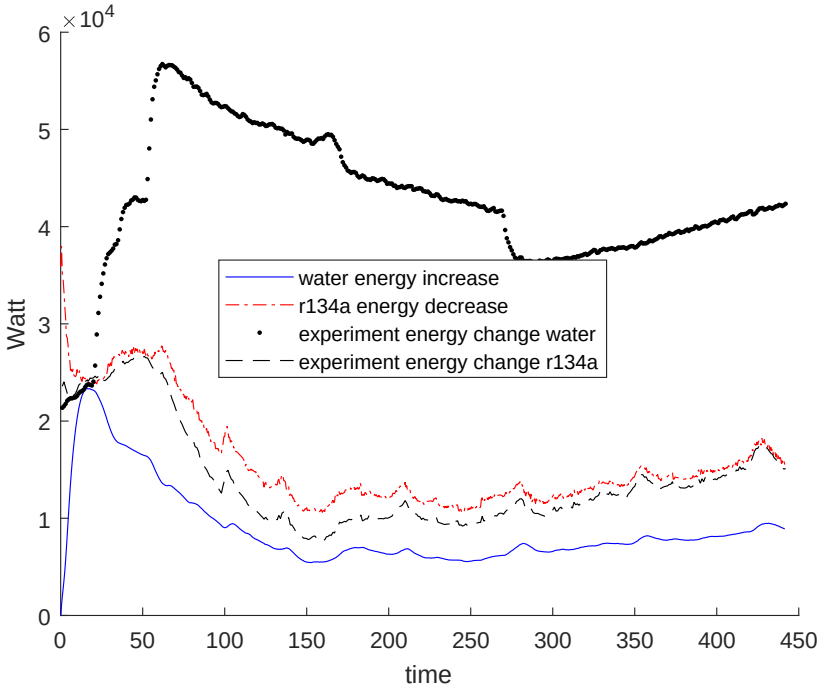


Figure 4.35. Condenser energy balance (second case)

The evaporator side outlet temperatures obtained in the simulations are presented in Figure 4.32, and the evaporator energy balance combined with the estimated heat transfer rate is shown in Figure 4.33. The condenser side outlet temperatures and the condenser energy balance are presented Figure 4.34 and Figure 4.35, respectively.

The results show that the outputs obtained via the numerical simulations reflect the behavior of the transient action reasonably well. There are many effects on the real life experiment which have not and possible can not be incorporated numerical model. Moreover, the experimental ORC system never fully reached the steady state condition, as some inputs varied constantly during the process; therefore, similar transient response from numerical and experimental simulation is more likely to be expected rather than perfectly overlapping temperature outputs. Another reason for the temperature difference can be explained by locations of the thermal sensors. It may expected that the working fluid would get colder between exiting the evaporator and reaching the thermal sensor. In addition, there is reason to suspect that the mass flow rates of the experiment have not been measured accurately, and this error would, if it

were indeed present, help to explain the difference between the energy balance curves derived from the experiment. To sum up, we conclude that the numerical model represents the transient behavior reasonably and numerical simulations do not deviate dramatically from real life results. In the next chapter a numerical simulation of ORC system will be presented based on previously introduced model.

# 5. SIMULATION OF AN ORC SYSTEM

The construction of the numerical model and the examination of the outputs based on the experimental data is presented in the previous chapters. In this chapter the simulation of the ORC system will be presented.

## 5.1. Inputs of the simulation

The numerical model is constructed similar to the ORC in the BURET Laboratory. Therefore, the time dependent variables of the numerical system are also the variables, that are controllable in the experimental setup. The time dependent variables of the ORC are the system pressure, hot oil (renolin) inlet temperature, cold water inlet temperature, cold water mass flow rate and the working fluid's (r134a) mass flow rate. The time histories of those variables defined before the simulation begins. The simulation first assures evaporation ($0-200$th seconds), than by changing the inputs it reaches different steady state conditions, at last it returns to the second steady state condition where the increase of the temperature and the system pressure began. At the 900th second, the temperature of the cooling water decreased and the mass flow rate of the cooling water increased to observe the similar transient response of the refrigerant's mass flow rate with the study of Lee *et al.* [8]. The time independent variables are selected as their values in the experimental setup. Figure 5.1 shows the time histories of the hot oil and cold water inlet temperatures. Figure 5.2 shows the mass flow rate time histories of the working fluid and cold water. Figure 5.3 shows the system pressure time history. The simulation scenerio is presented in the Table 5.1 and Table 5.2. The sigmoid function is employed for the time dependent transition of the input variables. The time step is 0.01 seconds and the discretization of the heat exchangers is made with 30 subcells.

Table 5.1. Inputs 0-800

| **Time span [s]** | **0-200** | **200-400** | **400-600** | **600-800** |
|---|---|---|---|---|
| **Sys. Pressure [bars]** | 8 | 10 | 15 | 19 |
| **Ref. Mass Flow Rate [kg/s]** | 0.1 | 0.1 | 0.15 | 0.2 |
| **Oil Inlet Temperature [C]** | 60 | 65 | 75 | 90 |
| **Water Inlet Temperature [C]** | 8 | 8 | 8 | 8 |
| **Water Mass Flow Rate [kg/s]** | 0.8 | 0.8 | 0.8 | 1 |

Table 5.2. Inputs 800-1200

| **Time span [s]** | **800-900** | **900-1000** | **1000-1200** |
|---|---|---|---|
| **Sys. Pressure [bars]** | 15 | 15 | 10 |
| **Ref. Mass Flow Rate [kg/s]** | 0.15 | 0.15 | 0.1 |
| **Oil Inlet Temperature [C]** | 95 | 75 | 65 |
| **Water Inlet Temperature [C]** | 8 | 6 | 10 |
| **Water Mass Flow Rate [kg/s]** | 0.8 | 1.2 | 0.6 |

The time independent inputs of the ORC simulation are as follows:

- Hot oil mass flow rate = 1.6 kg/s
- Hot oil pressure = 1 bar
- Water pressure = 1 bar
- Initial temperature (at $t = 0$) of the working fluid = 12 Celsius
- The system pressure after the expander = 7 bars

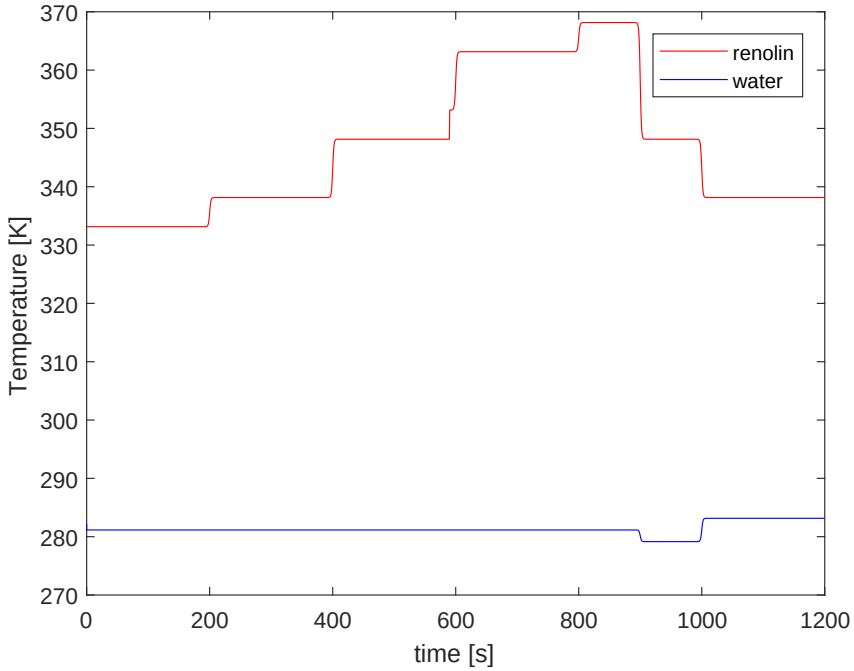


Figure 5.1. Inlet temperature time histories

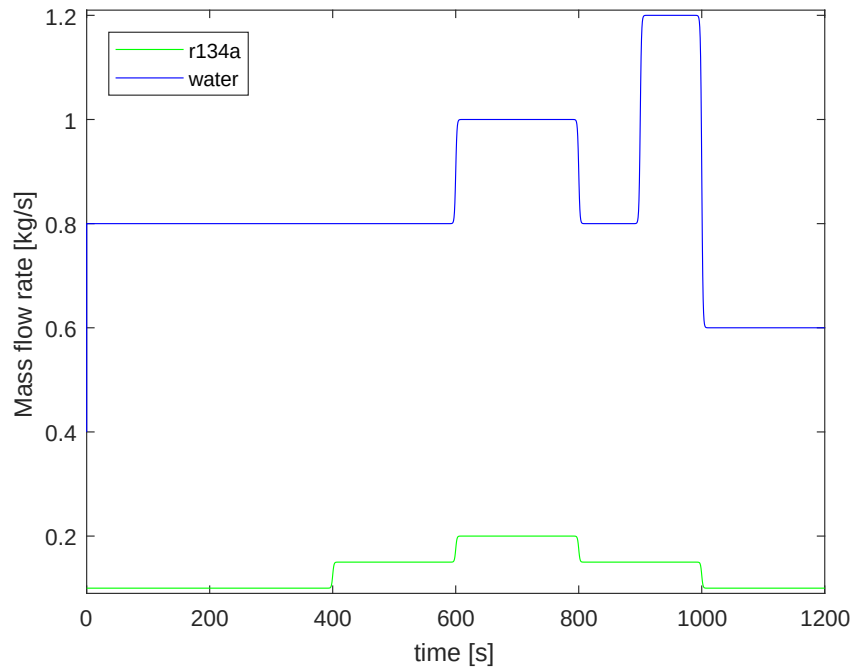


Figure 5.2. Mass flow rate time histories

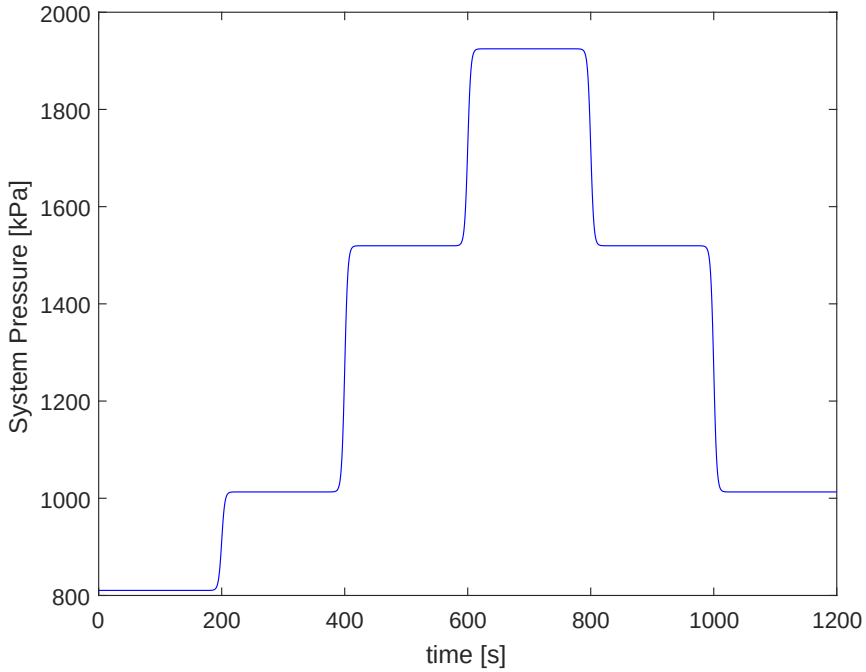


Figure 5.3. System pressure time history

## 5.2. Results of the Simulation

The estimated work output of the ORC simulation is calculated by the steady state formulation of the expander. It's time history is shown in the Figure 5.4. The inlet temperature of hot oil, and the evaporator's inlet and outlet temperatures of the refrigerant side, combined with the system pressure, time histories are represented in Figure 5.5. The condenser's refrigerant side inlet and outlet temperatures, cooling water inlet temperature and cooling water mass flow rate time histories are given in Figure 5.6. The energy balances of the evaporator and the condenser are given in Figures 5.7 and 5.8 respectively. The enclosed mass time histories are shown in Figure 5.9. Inlet and outlet mass flow rate time histories of the evaporator and the condenser are given in Figures 5.10 and 5.11 respectively.

## 5.3. Remarks to the Simulation

The duration of the simulation is 1200 seconds. During the process, six steady state conditions are reached. The first indicator of being in steady state is the equality

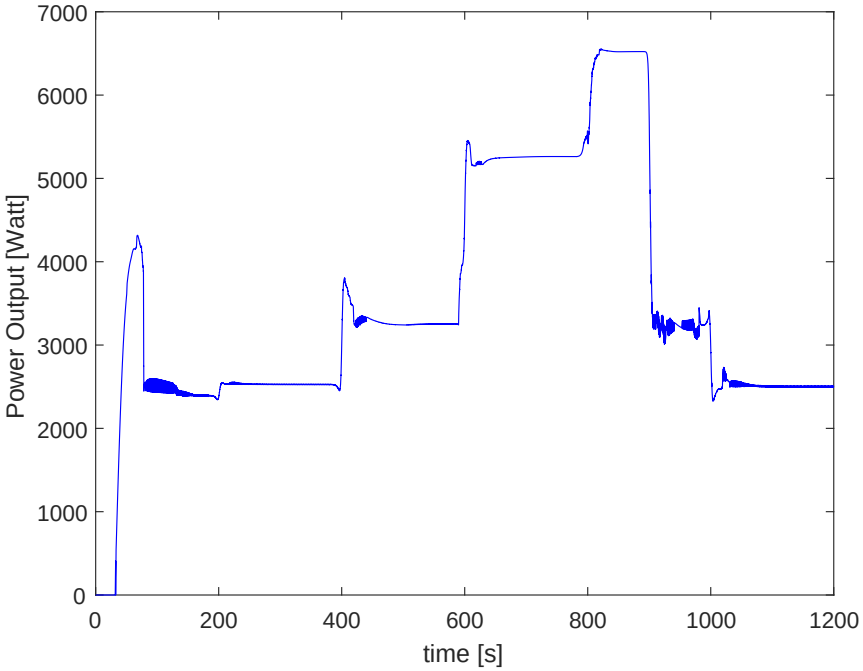


Figure 5.4. Work output time history

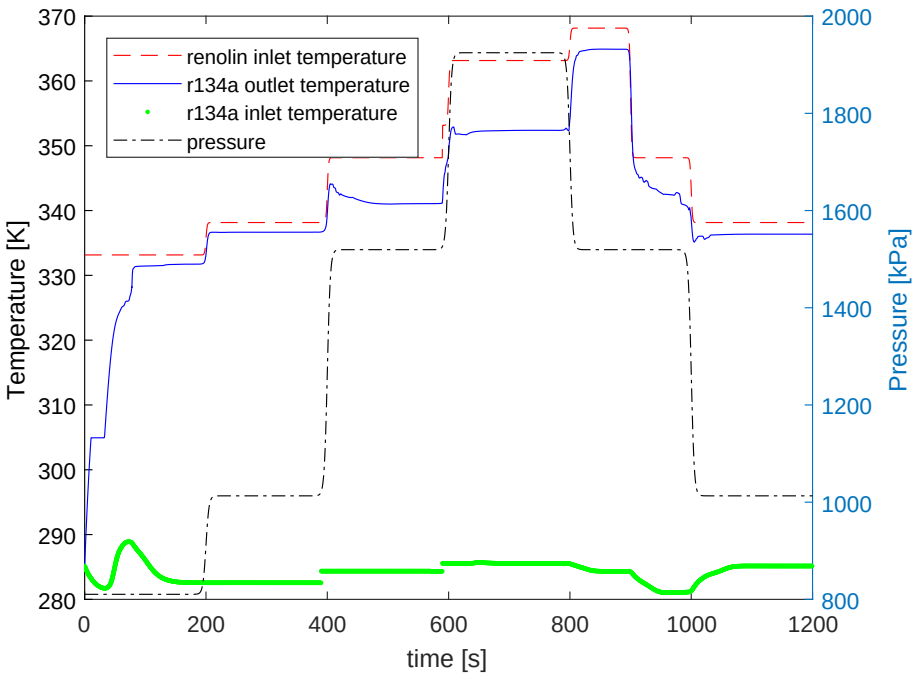


Figure 5.5. Evaporator side temperatures vs time

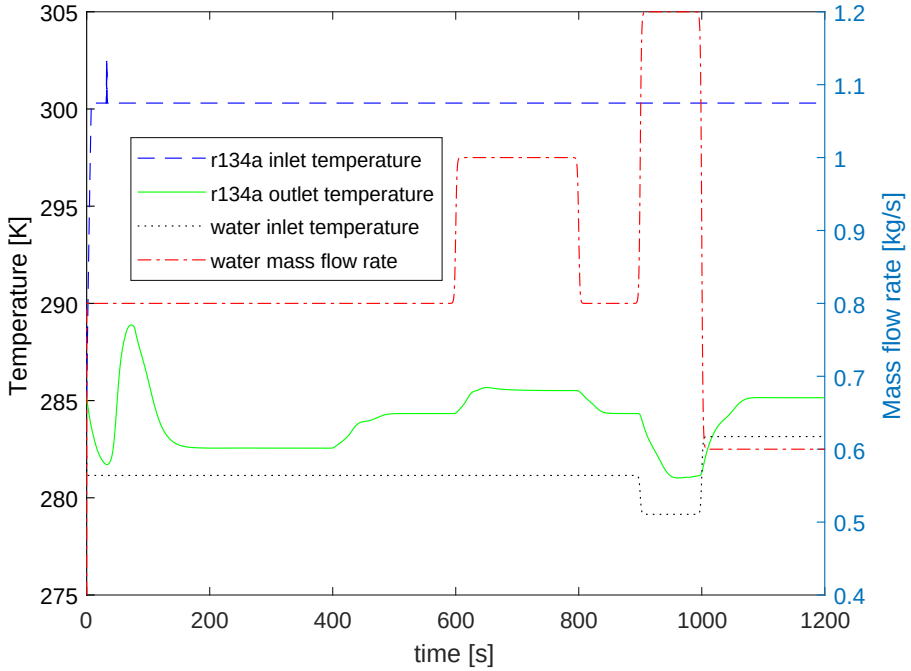


Figure 5.6. Condenser side temperatures vs time

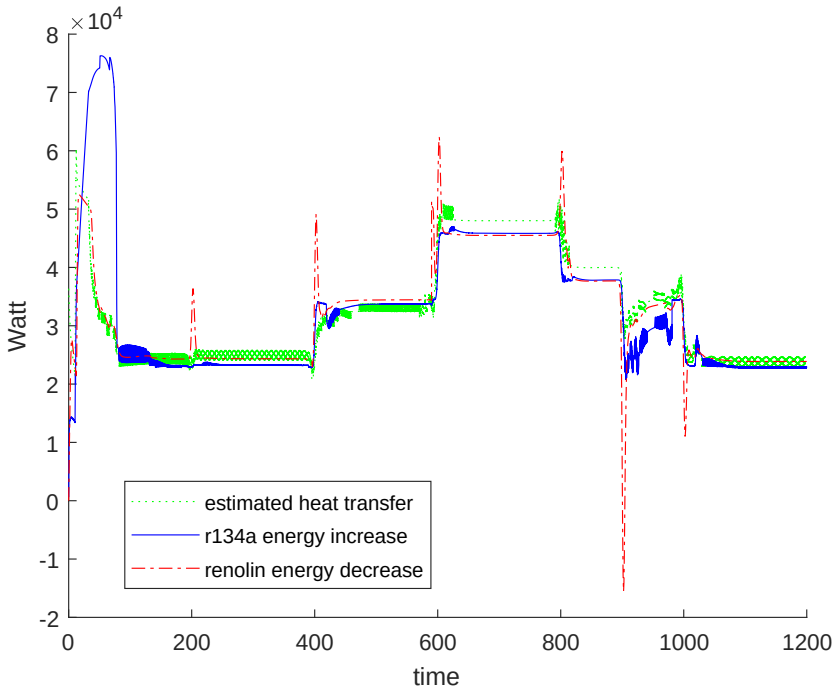


Figure 5.7. Evaporator energy balance time history

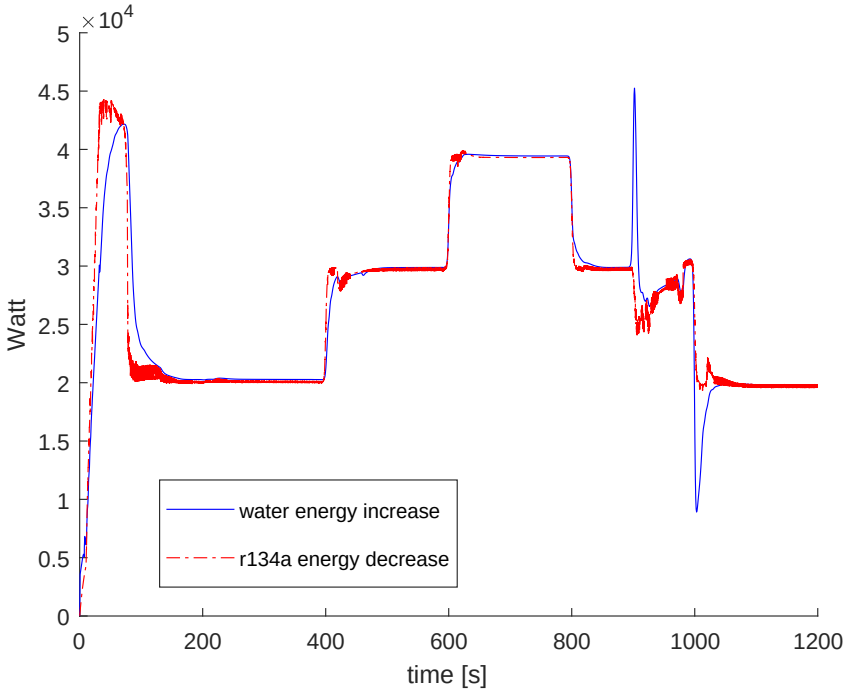


Figure 5.8. Condenser energy balance time history

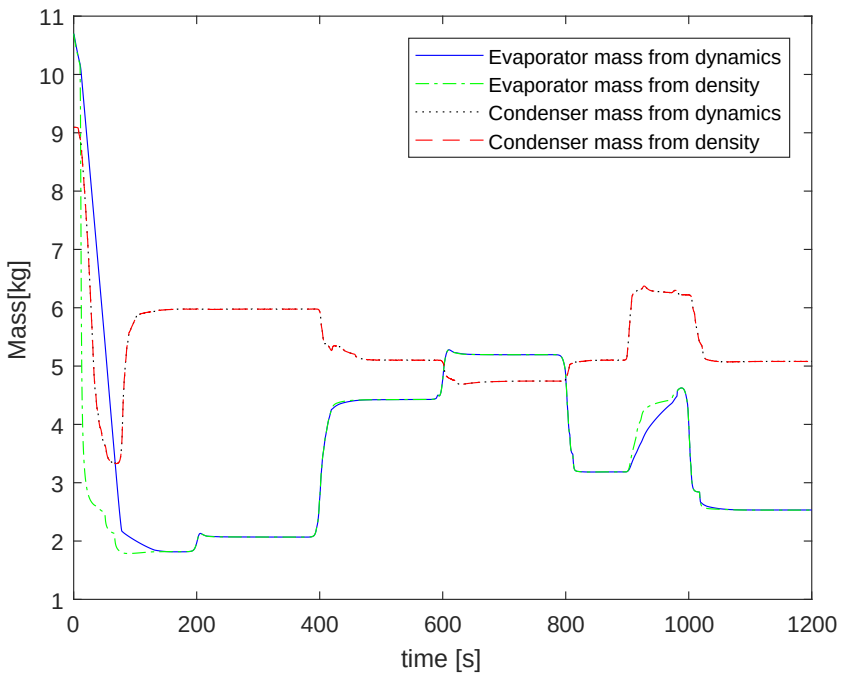


Figure 5.9. Enclosed mass by heat exchangers vs time

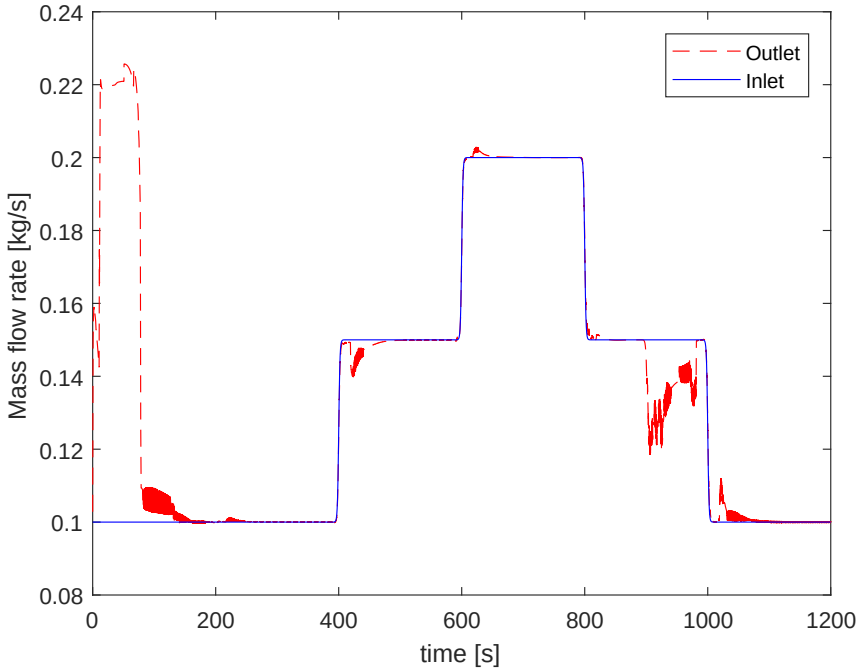


Figure 5.10. Evaporator mass flow rate vs time

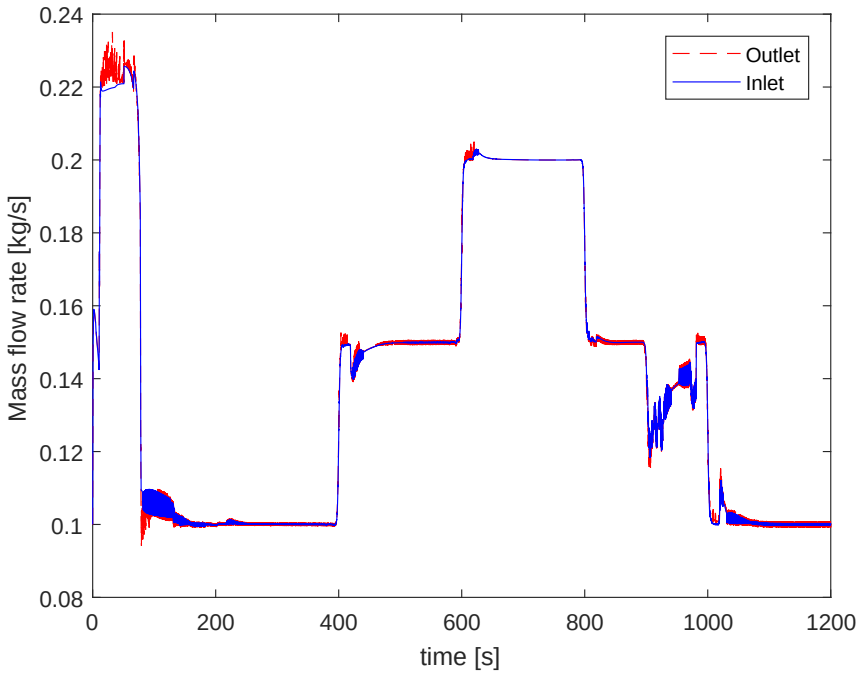


Figure 5.11. Condenser mass flow rate vs time

of inlet and outlet mass flow rates for each heat exchanger. Another one is the equality of inlet and outlet energy differences of both fluids. The energy balance chart of the evaporator is supported by the heat transfer rate. In the steady state the inlet and outlet energy differences of the fluids are near to the estimated heat transfer rate.

There are two important observations based on the results, first one is observed in the power output chart around 90th second. The working fluid was in it's liquid phase at the beginning, the evaporation process increases mass flow rate at the exit of the evaporator and the increased mass flow rate causes a peak in the power generation. The power generation decreases when evaporation is over and system becomes steady. The second important observation is at 900th second, the system variables changed in the way, that system's heat input is lowered and the chilling effect of the water is increased. This led a choking effect on the mass flow rate and reduced the power generation significantly. This observation is parallel to the transient response obtained by Lee *et al.* [8].

The simulation scenerio may be rearrenged as a future work, to observe the transient effects of the each variable on the system. Moreover a controller algorithm may be implemented, and, the power generation may be kept in a constant level.

# 6. CONCLUSION

A numerical dynamic model is constructed for an ORC system. The constructed model represents transient outcomes similar to the real life experimental results. Some assumptions are made for simplification of the model. The key ones are that there is no pressure loss due to the frictional forces, and the density of the working fluid changes instantly due to changing pressure. Apart from the assumptions, numerical model obeys mass and energy conservation rules and shows a small deviation from momentum balance when flow is in two phase.

The inputs of an ORC system is defined and simulations are made to see the transient response according to changing inputs. The numerical model is constructed in MATLAB in such a way that one can easily change utilized heat transfer correlations, number of subcells, the geometry of the heat exchanger, the working fluid in the system (limited by thermodynamic state library -REFPROP-). Therefore the constructed model is open to any maintenance and refinement. It is also flexible to the changing boundary values. Moreover some filters are formulated in the system to increase stability and a quasi-dynamic version is also introduced in the model to perform quick simulations based on energy balance formula to see the behaviour rapidly.

The model has variable spatial distribution of the mass flow rate through the heat exchanger. Many dynamic models available in the literature have constant mass flow rate. Having variable mass flow rate increases the accuracy of the transient response and indicates whether or not system is in the steady state.

The model is still developing and there are many physical phenomena which need to be modeled in more detail. For example the pressure dependent transients are need to be implemented in the system for more accuracy in the future studies. The heat exchanger library can be expanded and more correlations may be introduced as a further study. Moreover, turbine and pump dynamics may also be included for more realistic simulations. A control algorithm can also be utilized for manipulating

some variables, so that system achieve optimal steady state operating condition. Apart from model maintenance, a study based on this model can be conducted to define and achieve a optimal working condition for any input.

# REFERENCES


1. Wei, D., X. Lu, Z. Lu and J. Gu, "Performance analysis and optimization of organic Rankine cycle (ORC) for waste heat recovery", *Energy Conversion and Management*, Vol. 48, No. 4, pp. 1113 – 1119, 2007.

2. Gnielinski, V., "New equations for heat and mass transfer in the turbulent flow in pipes and channels", *NASA STI/Recon Technical Report A*, Vol. 75, pp. 8–16, 1975.

3. The Association of German Engineers - Chemical and Process Engineering, *VDI-Wärmeatlas*, VDI-Wärmeatlas, Springer Berlin Heidelberg, 2013.

4. Quoilin, S., R. Aumann, A. Grill, A. Schuster, V. Lemort and H. Spliethof, "Dynamic modeling and optimal control strategy of waste heat recovery Organic Rankine Cycles", *Applied Energy*, Vol. 88, pp. 2183–2190, 2011.

5. Vaja, I., *Definition of an object oriented library for the dynamic simulation of advanced energy systems: methodologies, tools and application to combined ICE-ORC power plants*, Ph.D. Thesis, Università di Parma, Dipartimento di Ingegneria Industriale, 2009.

6. Twomey, B. L., *Dynamic simulation and experimental validation of an Organic Rankine Cycle model*, Ph.D. Thesis, The University of Queensland, School of Mechanical and Mining Engineering, 2016.

7. Bracco, R., S. Clemente, D. Micheli and M. Reini, "Experimental tests and modelization of a domestic-scale ORC (Organic Rankine Cycle)", *Energy*, Vol. 58, No. Supplement C, pp. 107 – 116, 2013.

8. Lee, Y.-R., C.-R. Kuo and C.-C. Wang, "Transient response of a 50 kW organic Rankine cycle system", *Energy*, Vol. 48, No. 1, pp. 532 – 538, 2012, 6th Dubrovnik

Conference on Sustainable Development of Energy Water and Environmental Systems, SDEWES 2011.

9. Zhang, J., W. Zhang, G. Hou and F. Fang, "Dynamic modeling and multivariable control of organic Rankine cycles in waste heat utilizing processes", *Computers & Mathematics with Applications*, Vol. 64, No. 5, pp. 908 – 921, 2012, advanced Technologies in Computer, Consumer and Control.

10. Colonna, P. and H. van Putten, "Dynamic modeling of steam power cycles.: Part I—Modeling paradigm and validation", *Applied Thermal Engineering*, Vol. 27, No. 2, pp. 467 – 480, 2007.

11. van Putten, H. and P. Colonna, "Dynamic modeling of steam power cycles: Part II – Simulation of a small simple Rankine cycle system", Vol. 27, pp. 2566–2582, 10 2007.

12. Li, B. and A. Alleyne, "A dynamic model of a vapor compression cycle with shutdown and start-up operations", *International Journal of Refrigeration*, Vol. 33, No. 3, pp. 538–552, 5 2010.

13. McKinley, T. and A. Alleyne, "An advanced nonlinear switched heat exchanger model for vapor compression cycles using the moving-boundary method", *International Journal of Refrigeration*, Vol. 31, No. 7, pp. 1253–1264, 11 2008.

14. Casella, F., F. Donida and J. Akesson, "Object-Oriented Modeling and Optimal Control: A Case Study in Power Plant Start-Up", *Preprints of the 18th IFAC World Congress*, 2011.

15. Bamgbopa, M. O. and E. Uzgoren, "Quasi-dynamic model for an organic Rankine cycle", Vol. 72, pp. 117 – 124, 08 2013.

16. Espinosa, N., I. Gil-Roman, D. Didiot, V. Lemort, B. Lombard and S. Quoilin, "Transient Organic Rankine Cycle Modelling for Waste Heat Recovery on a Truck",

*24th International Conference on Efficiency, Cost, Optimization, Simulation and Environmental Impact of Energy Systems*, 2011.

17. Ziviani, D., A. Beyene and M. Venturini, "Advances and challenges in ORC systems modeling for low grade thermal energy recovery", *Applied Energy*, Vol. 121, pp. 79–95, 2014.

18. Chowdhury, J. I., B. K. Nguyen and D. Thornhill, "Dynamic model of supercritical organic rankine cycle waste heat recovery system for internal combustion engine", *International Journal of Automative Technology*, Vol. 18, pp. 589–601, 2017.

19. Ansari, M. R. and V. Mortazari, "Simulation of dynamical response of a counter-current heat exchanger to inlet temperature or mass flow rate change", *Applied Thermal Engineering*, Vol. 26, pp. 2401–2408, 2006.

20. Al-Dawery, S. K., A. M. Alrahawi and K. M. Al-Zobai, "Dynamic modeling and control of plate heat exchanger", *International Journal of Heat and Mass Transfer*, Vol. 55, No. 23, pp. 6873 – 6880, 2012.

21. Ebrahimzadeh, E., P. Wilding, D. Frankman, F. Fazlollahi and L. L. Baxter, "Theoretical and experimental analysis of dynamic plate heat exchanger: Non-retrofit configuration", *Applied Thermal Engineering*, Vol. 93, pp. 1006–1019, 2016.

22. Jensen, J. M. and H. Tummescheit, "Moving Boundary Models for Dynamic Simulations of Two-Phase Flows", *2nd International Modelica Conference*, 2002.

23. Willatzen, M., N. B. O. L. Pettit and L. Ploug-Sorensen, "A general dynamic simulation model for evaporators and condensers in refrigeration. Part I: moving-boundary formulation of two-phase flows with heat exchange", *International Journal of Refrigeration*, Vol. 21, pp. 398–403, 1998.

24. Willatzen, M., N. B. O. L. Pettit and L. Ploug-Sorensen, "A general dynamic simulation model for evaporators and condensers in refrigeration. Part II: simulation

and control of an evaporator", *International Journal of Refrigeration*, Vol. 21, pp. 404–414, 1998.

25. Garcia-Valladares, O., "Numerical simulation of triple concentric-tube heat exchangers", *International Journal of Thermal Sciences*, Vol. 43, pp. 979–991, 2004.

26. Xuan, S., V. Aute and R. Radermacher, "Generic Dynamic Model for Heat Exchangers", *International Refrigeration and Air Conditioning Conference*, 2006.

27. Bracco, S., I. Faccioli and M. Troilo, "A Numerical Discretization Method for the Dynamic Simulation of a Double-Pipe Heat Exchanger", *International Journal of Energy*, Vol. 1, 2007.

28. Zhao, Y., Y. Liang, Y. Sun and J. Chen, "Development of a mini-channel evaporator model using R1234yf as working fluid", *International Journal of Refrigeration*, Vol. 35, pp. 2166–2178, 2012.

29. Klimenko, V. V., "A generalized correlation for two-phase forced flow heat transfer - second assessment", *International Journal of Heat and Mass Transfer*, Vol. 33, pp. 2073–2088, 1990.

30. Admiraal, D. M. and C. Bullard, *Heat transfer in refrigerator condensers and evaporators*, Tech. rep., Air Conditioning and Refrigeration Center. College of Engineering. University of Illinois at Urbana-Champaign., 1993.

31. Yan, Y. and T.-F. Lin, "Evaporation Heat Transfer and Pressure Drop of Refrigerant R134a in a Small Pipe", *Journal of Heat Transfer - Transactions of The Asme*, Vol. 121, pp. 118–127, 1999.

32. Ayub, Z. H., "Plate Heat Exchanger Literature Survey and New Heat Transfer and Pressure Drop Correlations for Refrigerant Evaporators", *Heat Transfer Engineering*, Vol. 33, pp. 3–16, 2003.

33. Palm, B. and J. Claesson, "Plate Heat Exchangers: Calculations Methods for Single- and Two-Phase Flow", *Heat Transfer Engineering*, Vol. 27, pp. 88–98, 2006.

34. Galeazzo, F. C., R. Y. Miura, J. A. Gut and C. C. Tadini, "Experimental and numerical heat transfer in a plate heat exchanger", *Chemical Engineering Science*, Vol. 61, No. 21, pp. 7133 – 7138, 2006.

35. Garcia-Cascales, J. R., F. Vera-Garcia, J. M. Corberan-Salvador and J. Gonzalvez-Macia, "Assessment of boiling and condensation heat transfer correlations in the modelling of plate heat exchangers", *International Journal of Refrigeration*, Vol. 30, pp. 1029–1041, 2007.

36. Chisholm, D. and A. S. Wanniarachchi, "Maldistribution in single-pass mixed-channel plate heat exchangers", *ASME HTD Compact Heat Exchangers for Power and Process Industries*, pp. 95–99, 1992.

37. Kakac, S. and H. Liu, *Heat Exchangers Selection, Rating and Thermal Design 2nd Edition*, CRC Press, 2002.

38. Martin, H., "A theoretical approach to predict the performance of chevron-type plate heat exchangers", *Chemical Engineering and Processing: Process Intensification*, Vol. 35, No. 4, pp. 301 – 310, 1996.

39. Djordjevic, E. and S. Kabelac, "Flow boiling of R134a and ammonia in a plate heat exchanger", *International Journal of Heat and Mass Transfer*, Vol. 51, pp. 6235–6242, 2008.

40. Khan, T. S., M. S. Khan, M.-C. Chyu, Z. H. Ayub and J. A. Chattha, "Review of Heat Transfer and Pressure Drop Correlations for Evaporation of Fluid Flow in Plate Heat Exchangers (RP-1352)", *HVAC&R Research*, Vol. 15, No. 2, pp. 169–188, 2009.

41. Abu-Khader, M. M., "Plate heat exchangers: Recent advances", *Renewable and Sustainable Energy Reviews*, Vol. 16, pp. 1883–1891, 2012.

42. Moran, M. J. and H. N. Shapiro, *Fundamentals of Engineering Thermodynamics*, Wiley, 2006.

43. Incropera, F. P. and D. P. DeWitt, *Introduction to Heat Transfer 4th Edition*, Wiley, 2001.

44. Shah, R. K. and D. P. Sekulic, *Fundamentals of Heat Exchanger Design*, Wiley, 2003.

45. Tovazhnyanski, L., P. Kapustenko and V. Tsibulnik, "Heat transfer and hydraulic resistance in channels of plate heat exchangers", *Energetika*, Vol. 9, pp. 123–125, 1980.

46. Gungor, K. and R. Winterton, "A general correlation for flow boiling in tubes and annuli", *International Journal of Heat and Mass Transfer*, Vol. 29, No. 3, pp. 351 – 358, 1986.

47. Shah, M., "Chart correlation for saturated boiling heat transfer: Equations and further study", *ASHRAE Transactions*, Vol. 88, 1982.